UTCM

"Improving the Quality of Life by Enhancing Mobility"

University Transportation Center for Mobility

DOT Grant No. DTRT06-G-0044

Methodology and Guidelines for Regulating Traffic Flows under Air Quality Constraints in Metropolitan Areas

Final Report

Yunlong Zhang, Qi Ying, Jinpeng Lv, and Sri Harsha Kota

Performing Organization
University Transportation Center for Mobility
Texas Transportation Institute
The Texas A&M University System
College Station, TX

Sponsoring Agency
Department of Transportation
Research and Innovative Technology Administration
Washington, DC

Texas Transportation Institute

UTCM Project #08-04-17
February 2010

Technical Report Documentation Page

1. Project No. UTCM 08-35-17	2. Government Accession No.	3. Recipient's Catalog No.
4. Title and Subtitle Methodology and Guidelines for Regulating Traffic Flows under Air Quality Constraints in Metropolitan Areas		5. Report Date February 2010 6. Performing Organization Code Texas Transportation Institute
7. Author(s) Yunlong Zhang, Qi Ying, Jinpeng Lv, and Sri Harsha Kota		8. Performing Organization Report No. UTCM 08-34-17
9. Performing Organization Name and Address University Transportation Center for Mobility™ Texas Transportation Institute The Texas A&M University System 3135 TAMU College Station, TX 77843-3135		10. Work Unit No. (TRAIS) 11. Contract or Grant No. DTRT06-G-0044
12. Sponsoring Agency Name and Address Department of Transportation Research and Innovative Technology Administration 400 7th Street, SW Washington, DC 20590		13. Type of Report and Period Covered Final Report January 2008 – December 2009 14. Sponsoring Agency Code

15. Supplementary Notes

Supported by a grant from the US Department of Transportation, University Transportation Centers Program

16. Abstract

This project developed a methodology to couple a new pollutant dispersion model with a traffic assignment process to contain air pollution while maximizing mobility. The overall objective of the air quality modeling part of the project is to develop a model to predict the air quality at receptor sites in metropolitan areas using traffic data from a coupled traffic model and real time meteorological data. Most of the air dispersion models in use do not have a full description of the physical and chemical processes to describe the formation and transformation of pollutants in the metropolitan areas relating to traffic flow and thus cannot provide complete information that is necessary in traffic planning and regulating. The reactive dispersion air quality model developed in this project includes a state-of-the-art gas chemistry mechanism (Statewide Air Pollution Research Center, or SAPRC, model) to predict the ozone, NOx, CO, benzene, acetaldehyde, formaldehyde and 1,3-butadine concentrations, and a complete particulate matter module with thermal dynamics to predict the concentrations of primary and secondary particulate pollutants including diesel particulate matter. With the air quality model developed in this project, traffic assignments can be conducted taking air quality into account. The air quality can be considered as a form of constraint that limits the pollutants under certain acceptable levels in parts of the transportation network. This consideration will be an added constraint in addition to the roadway segment capacity constraint in the assignment process. The air quality can also be considered as an additional objective function while assigning traffic flow in the metropolitan transportation network.

17. Key Word Air quality management, Metropolitan areas, Traffic assignment, Traffic flow	18. Distribution Statement Public distribution		
19. Security Classif. (of this report) Unclassified	20. Security Classif. (of this page) Unclassified	21. No. of Pages 87	22. Price n/a

Methodology and Guidelines for Regulating Traffic Flows under Air Quality Constraints in Metropolitan Areas

by

Yunlong Zhang

Qi Ying

Jinpeng Lv

Sri Harsha Kota

University Transportation Center for Mobility™

Texas Transportation Institute

The Texas A&M University System

3135 TAMU

College Station, TX 77843-3135

February 2010

DISCLAIMER

ACKNOWLEDGMENTS

Support for this research was provided in part by a grant from the U.S. Department of Transportation, University Transportation Centers Program to the University Transportation Center for Mobility™ (DTRT06-G-0044).

TABLE OF CONTENTS

LIST OF FIGURES

LIST OF TABLES

EXECUTIVE SUMMARY

According to air quality data published by the U.S. Environmental Protection Agency (EPA) (http://www.epa.gov/air/data/geosel.html), monitored pollutant concentrations exceed the limits of the National Ambient Air Quality Standards (NAAQS) in many metropolitan areas. Areas that have failed to meet federal standards for ambient air quality are designated as nonattainment areas. In Texas, nonattainment areas include Houston–Galveston–Brazoria (HGB), Dallas–Fort Worth (DFW), Beaumont–Port Arthur (BPA), San Antonio (SA), and El Paso (ELP).

In a metropolitan area, air pollutant concentrations are significant largely due to heavy traffic flows and traffic congestion. Therefore, "hot spots" of air pollution form in some areas of metropolitan locations. Once concentrations exceed required limits, it is difficult to adjust the traffic flows to comply with the air quality standards. Therefore, it is necessary and very beneficial to develop strategies during the planning stage to regulate traffic flows and comply with air quality standards. These strategies should consider the impacts of traffic flow, land use, traffic management, and air quality control. This is especially important for sensitive and large-exposure locations such as hospitals, schools, and gas stations in heavy traffic areas.

Regulating traffic flows under air quality constraints in metropolitan areas depends strongly on the development of near-road dispersion and traffic assignment models. This study aimed to move the development of both of these two models forward. In this report, the Eulerian equation and its solution were presented first; then General Motors (GM) data were used to model pollutant dispersion, and the gas phase chemistry was considered. The numerical studies suggested that gas phase chemistry was needed to accurately predict the concentration of ozone (O_3), nitric oxide (NO), nitrogen dioxide (NO_2), and 1,3-Butadiene (BUTA). The effect of gas phase chemistry on BUTA was less significant when the freeway was in an O_3-depleted location, such as an urban center, but was quite significant when the freeway was located downwind of the urban ozone plume due to a significant increase in the hydroxyl oxide (HO) concentration. Neglecting the gas chemistry near freeways would lead to an overestimation of ozone-rich air toxins in the downwind direction. In addition, the increase in the HO radical near freeways might imply potential health effects due to the strong oxidative power of the radicals.

On the other hand, in developing the traffic assignment model, an optimization problem was formulated. The objective function was established to represent the total travel cost, and the constraints concern the three requirements of traffic demand, travel speeds, and emission levels. CO was chosen to form the emission constraints because it is very stable and involves few chemical reactions. Simulations were run in a network in College Station, Texas, involving 6 nodes, 14 links, and 74 paths. The tradeoff between the travel cost and air quality was examined by tracking the evolution of the optimal objective value (total travel time) with the change in emission constraints (CO concentrations). The air quality benefit from relocating traffic was identified by an observed 13.3% reduction in the emission level with only 2.1% increase in total travel time. In addition, two other emissions, NO_2 and O_3, were evaluated under different sets of link volumes. Simulation results indicated that NO_2 followed a similar trend of CO concentration evolution. However, there was no significant spatial difference in the highest O_3 concentrations among different sets of link volumes because O_3 involves very complex chemical reactions. As an emission type involved more complex chemical reactions, the highest concentration value of the emission type became more dependent on the total traffic in the study area instead of the traffic assignment within the network.

In the last chapter of this report, authors discuss the potential research directions indicated by this study. First, the models need to be calibrated and validated considering the changes of vehicle engines and driver behaviors over time; second, emissions involving chemical reactions to different degrees (e.g., CO, NO_2, and O_3) are expected to be considered in the optimization problem simultaneously; third, a more accurate estimation of vehicle movements in the network could move forward application of the proposed model at the operation level.

1. INTRODUCTION

1.1. Air Pollution Due to Vehicle Emissions

Vehicles on roadways emit a significant amount of air pollutants into the atmosphere. The pollutants emitted directly from vehicles include CO, nitrogen oxides (NO_x), volatile organic compounds (VOC), and fine and ultrafine particulate matter (PM). Air quality monitoring studies have detected elevated concentrations of these compounds within a short distance from freeways. For example, Grosjean et al. (2001) studied the concentration of carbonyls in a four-lane tunnel in Pennsylvania and reported a concentration of 16.44 $\mu g/m^3$; Murena (2007) analyzed benzene, toluene, ethyl benzene, and xylene (BTEX) compounds near a three-lane road in Italy and reported concentrations of 21.6, 318.9,121.2, and 541.5 $\mu g/m^3$, respectively; Kean et al. (2000) observed concentrations of ammonia and carbon dioxide (CO_2) of about 0.384 and 1081 ppm, respectively, near the Caldecott tunnel on Highway 24 in Berkeley, California; and Zhu et al. (2002) observed the concentration of black carbon and carbon monoxide in the range of 20.3–24.8 $\mu g/m^3$ and 1.9–2.6 ppm, respectively, near I-710 at the Los Amigos County Club in California.

Brugge et al. (2007) estimated that about 11% of people live within 100 m of a freeway in the United States. Richmond-Bryant et al. (2009) reported that school children were being exposed to high concentrations of particulate matter less than 2.5 micrometers in diameter ($PM_{2.5}$) and black carbon, 150.5 and 8.4 $\mu g/m^3$, respectively, at a street canyon in New York. Various studies have shown that adverse health effects are associated with traffic-related air pollution. Some of them are discussed below.

Kim et al. (2004) observed a clear relation between respiratory diseases and children attending and living near schools located in busy traffic areas in California. Gauderman et al. (2007) showed that freeway pollution had a substantial impact on the lung development of children in the age group of 8–18 years. Findings revealed that the lung deficiencies in children living in the range of 500 m from a freeway were more than the ones living 1200 m away. Finkelstein et al. (2004) studied the relation between the rate advancement period (i.e., premature mortality rate) in people and their living distance from a freeway. Results showed a rate advancement period of about 2.5 years for people living at 100 m from a highway.

Venn et al. (2001) showed that the risk of wheezing in children increased with a decreased distance from a road. Balmes et al. (2009) studied the relation between lung function in asthma-affected adults and traffic exposure, and showed that the exposure to any density of road traffic can play a pivotal role in deterioration of health.

Vehicle exhaust is one of the major contributors of greenhouse gases and thus global climate change. Niemeier et al. (2006) estimated that about 10–20% of present ozone radiative forcing was due to global road traffic emissions. Wade et al. (1994) estimated that about 60–70% of global warming due to vehicles was a result of carbon dioxide, and it is estimated that 1,887.4 million metric tons of CO_2 per year in the United States come from the transportation sector (U.S. EPA, 2009). Figure 1 shows the contribution of carbon dioxide from different sectors in the United States.

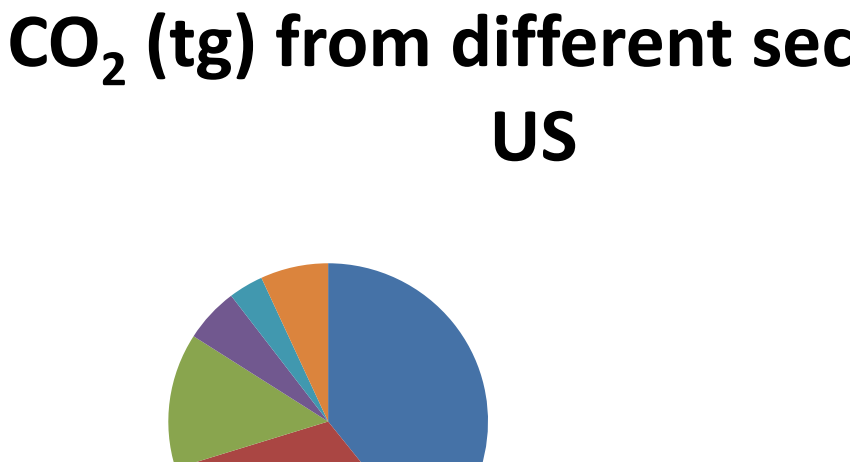

Figure 1. Percentage of carbon dioxide emitted from different sectors in the U.S., based on data from U.S. greenhouse gas emission inventory report (U.S. EPA, 2009)

1.2. Near-Road Dispersion Models

Numerical models are useful tools in understanding the transport and fate of air pollutants near freeways and are often used in exposure studies based on the predicted pollutant

concentrations. Models used in near-road studies vary from simple line source models for steady state dispersion of conservative tracers to full-fledged time-dependent grid models with simplified gas phase chemistry. The uniqueness of near-road models to general purpose atmospheric dispersion models is the turbulence caused by vehicle movement.

Sehmel (1973) used zinc sulfide (ZnS) tracer particles to study the re-suspension of particles due to moving traffic. Mass balance on the ZnS tracer particles measured by the downwind samplers showed that the turbulent transport of re-suspended particles depended on vehicular velocity. This vehicle-induced turbulence must be represented appropriately in the models to allow accurate dispersion calculations. Some of the modeling studies developed to study near-road air quality are discussed in detail below.

Benson (1992) developed a series of line source dispersion models, CALINE3 and CALINE4, based on the Gaussian line source dispersion equation. The highway link was divided into a series of equivalent finite line sources positioned normal to the wind direction. Each element was divided into three sub-elements whose geometry depended on road wind angle. The emission from each element was assumed to be the same. The mixing zone (zone above the freeway where the emissions and the turbulence are assumed to be uniform) was assumed to extend 3 m on either side of the travelled way. In addition to the solar heat flux, which accounts for the stability of atmosphere, an additional heat flux, which is formed due to movement of a vehicle, was used to estimate the stability class in the CALINE4 model. CALINE4 incorporated a simple chemical mechanism to simulate the concentration of reactive NO_2. The EPA used CALINE3 and CALINE4 for regulatory purposes before they were replaced by the American Meteorological Society and EPA Regulatory Model (AERMOD). This is a Gaussian short-range dispersion model developed especially for stationary sources, and it can be used for any terrain, but it does not account for vehicle-induced turbulence (Holmes and Morawska, 2006).

Held et al. (2003) developed a dispersion model (UCD, 2001) in which the highway link is divided into a three-dimensional (3D) array of point sources. The concentration of a pollutant at a location is the sum of pollutants dispersed from each of these point sources. A mixing zone, which extended 3 m laterally in each direction and extended 2.5 m in elevation, was used. Sulfur hexafluoride (SF6) concentrations near a simulated freeway at a GM testing facility were used to determine the model parameters and to evaluate the model performance.

The UCD 2001 model appears to have better performance than the CALINE 4 model.

Kinnee et al. (2004) used a geographical information system (GIS)-based approach to study the spatial distribution of pollutants from major roads in Houston. The traffic count data were overlaid on the road layer data in a GIS and interpolated along the length of the road to estimate the traffic flows along the road sections. The U.S. EPA's area source model, ISCST3, was used to evaluate the spatial distribution of benzene along the major roads in Harris County.

Venkatram et al. (2007) conducted a field study adjacent to I-440 in North Carolina to validate the dispersion parameterization used in a previously developed line source model (Venkatram, 2004). Traffic-related data were collected using a surveillance camera located 5 m from the freeway. Real time NO_x analyzers were located at 20 and 275 m downwind. Wind speed and direction were measured using a two-cup anemometer as well as four sonic anemometers located at 5, 20, and 100 m downwind of the freeway. The relation between wind speed and direction measured at sonic anemometers placed at different distances from the freeway showed significant vehicle-induced turbulence. Optical remote sensing instruments were set up parallel to the road at 7 and 17 m downwind of the freeway to study spatial average of NO concentration. The model performed well when the wind was parallel to the freeway, but the performance deteriorated as the wind direction changed to oblique.

Sahlodin et al. (2007) used a commercial computational fluid dynamics (CFD) model with moving traffic on a simulated freeway to estimate the vehicle-induced turbulent diffusion coefficients. The vehicle-induced turbulent diffusion coefficients were added to the atmospheric eddy diffusion coefficient to calculate the overall eddy diffusivity for a Gaussian dispersion model. The CFD calculated eddy diffusion coefficients were in general agreement with the values determined by Bäumer et al. (2005).

Rao (2002) developed a two-dimensional (2D) grid model called ROADWAY-2 that was based on the U.S. EPA's ROADWAY model. The wind, temperature, and eddy diffusivity fields were predicted online. The effect of vehicle wake on the turbulent diffusivity was parameterized using vegetation canopy flow theory. The ROADWAY-2 model was validated against the SF_6 data from the GM study. Although a simple chemistry mechanism for O_3 and NO_x was included, no details about the chemistry model and its application were discussed.

The ROADWAY-2 model is suitable for studies with a single freeway link but will have difficulty accommodating multiple highway links due to its 2D limitation.

1.3. Traffic Assignment with Air Quality Considerations

In the past decade, there have been some studies to control or reduce emissions by rerouting traffic. Benedek and Rilett (1998) modeled the environmental consideration using a nonconvex function between the link flow and the environmental cost. The vehicle emission rates were estimated by the software TRANSYT-7F. A numerical search method was used to identify the link flows for this optimization problem with nonconvex terms. In their case study, only a small difference of emissions was identified between the environmental consideration and the travel time consideration.

Nagurney et al. (1998) used the theory of variational inequalities to consider the cases of both compliance and noncompliance conditions for pollutants. The compliance condition was defined in this study as such that the pollutants generated by travelers were no more than the values held by their licenses. It was pointed out that the precisely allocated penalty could avoid over-emissions in the network. Nagurney (2000a) improved the previous work by developing alternative pollution permit systems. Furthermore, she identified three distinct emission paradoxes (Nagurney, 2000b). The first two cases were similar to the traditional concerns with the travel cost: the total emissions might be increased by adding a road or reducing the demands in the network. The last case suggested that the improvement of a road might increase the total emissions. These studies assumed a constant emission factor, which was used to compute the link emissions by multiplying the link volume (Nagurney et al., 1998; Nagurney, 2000a and 2000b).

Yin and Lawphongpanich (2006) focused on the conflict between alleviating congestions and reducing emissions. An optimization problem was formulated to minimize emissions. TRANSYT-7F was used to calibrate the coefficients in the emission function. Ahn and Rakha (2008) studied a real-world network with two nodes and two links. They concluded that the emission reduction was obtained when most drivers chose a slower arterial route instead of the highway route.

A recent study (Barth, 2007) aimed to create environmentally friendly navigation. Instead of using a shortest-distance or shortest-time algorithm, this study developed a set of cost functions of energy and emissions. Field data were collected to model the link-based emission factors. In the case study, two freeways of approximately the same distance competed with each other. Different traffic conditions, including free-flow, moderate congestion, and heavy congestion, were studied. The heavily congested route caused both the longest travel time and the highest fuel consumptions. However, surprisingly, the moderate congestion route, rather than the free-flow one, involved the lowest fuel consumption.

These studies on traffic assignment considering air quality considered only emissions produced on a link by the traffic on the same link and failed to consider link geometries and the superposition of emissions from multiple links. In reality, many vulnerable objects are under a combined influence of more than one link, and in many cases, more than one roadway.

1.4. Summary

Regulating traffic flows under air quality constraints in metropolitan areas is highly dependent on the developments of the near-road dispersion model and the traffic assignment model. In this study, we improved both of the models based on reviewing previous research work.

Near-Road Dispersion Model

Although significant progress has been made in the numerical simulation of near-freeway air pollution, much of the effort so far has been focused on pollutant dispersion. Little is known about the formation, destruction, and transformation of primary emitted pollutants in the near-road environment, due to the lack of a complete representation of the chemistry and physics. High concentrations of volatile organic compounds and NO_x in the near-road environment are expected to produce high concentrations of hydroxyl radicals and other intermediate free radicals during the day. This could potentially change the chemical composition of the air parcel as it travels downwind. Therefore, the primal goal of the first

part of this study was to develop a three-dimensional near-road air quality model with a modern gas phase photochemical mechanism that could be used to study the transport and physical/chemical transformation of gaseous pollutants in areas with multiple freeway links and other sources.

Traffic Assignment Model

The studies on traffic assignment considering air quality were developed over time and accepted by more and more researchers. However, there are primarily two drawbacks in these studies that limit their applications to assign traffic for planning purposes. First, most of them considered only emissions produced on a link by the traffic on the same link (Benedek and Rilett, 1998; Nagurney et al., 1998; Nagurney, 2000a, 2000b; Yin and Lawphongpanich, 2006; Barth, 2007; and Ahn and Rakha, 2008) and failed to consider the link geometries and the superposition of emissions from multiple links. In reality, many vulnerable objects are under the combined influence of more than one link, and in many cases, more than one roadway. In addition, an emission value for a link or network cannot identify the environmental impact of traffic on the locations that are some distances away from the road. Second, the recent studies tested their models only in small networks. In the work of Nagurney et al. (1998), Nagurney (2000a and 2000b), and Yin and Lawphongpanich (2006), the networks involved only several one-directional links; the studies by Barth (2007) and Ahn and Rakha (2008) considered only two competitive paths under a signal origin-destination (O-D) pair. The feasibility of applying these models to a large-scale network is still unclear. Thus, the objective of the second part of this study was to model the traffic assignment problem under air quality constraints for the planning purpose, efficiently solve it, and discuss its application in practice.

The remainder of this report was organized as follows. Chapter 2 modeled the near-road air quality. The Eulerian equation and its solution were presented first, then the GM data was used to model the pollutant dispersion, and, last, the gas phase chemistry was also considered. Chapter 3 modeled the traffic assignment with air quality considerations. A general optimization problem was formulated to consider both the traditional traffic requirement and the air quality requirement; specified methods were then discussed to identify the general terms in the optimization problem, and the physical/chemical transformation of gaseous pollutants was evaluated for different traffic assignment solutions. Finally, Chapter 4 provided concluding comments and suggests future research.

2. MODELING THE NEAR-ROAD AIR QUALITY

2.1. Description of the Near-Road Chemical Transport Model

2.1.1. General Chemical Transport Model Formulation

The reactive transport equation for species *i* in 3D Cartesian coordinates is given by Equation (1).

$$\frac{\partial C_i}{\partial t} = -\frac{\partial (UC_i)}{\partial x} - \frac{\partial (VC_i)}{\partial y} - \frac{\partial (WC_i)}{\partial z} + \frac{\partial}{\partial x}\left(K_{xx}\frac{\partial C_i}{\partial x}\right) + \frac{\partial}{\partial y}\left(K_{yy}\frac{\partial C_i}{\partial y}\right) + \frac{\partial}{\partial z}\left(K_{zz}\frac{\partial C_i}{\partial z}\right) + R_i + L_i + S \quad (1)$$

where U, V, and W indicate wind speed in x, y, and z directions, respectively; C denotes concentration of species *i*; K_{xx}, K_{yy}, and K_{zz} are the turbulent diffusivities in x, y, and z planes; R and L denote the rate of production and loss due to chemical reactions, respectively; and S is the emission rate of the species *i*.

Turbulence Parameterization

As observed in Section 1.2, even though studies in the vicinity of a roadway indicated that turbulence created by moving traffic plays an important role in the near-road diffusion of the pollutant, very few models explicitly included this additional turbulence created near a freeway. In the present study, we used a new parameterization developed by Bäumer et al. (2005) in a three-dimensional chemical transport model. In this parameterization scheme, the overall turbulent diffusivity near a freeway was assumed to be a linear summation of atmospheric and vehicle-created turbulent diffusivities, as shown in Equation (2).

$$K_{jj} = K_{jj,atm} + K_{jj,mw} \quad (2)$$

where $K_{jj,atm}$ is eddy diffusivity due to atmospheric turbulence, and $K_{jj,mw}$ is the additional eddy diffusivity due to vehicle-induced turbulence along the axis "j." The atmospheric turbulent diffusivity was determined based on the Monin-Obukhov similarity theory (Monin and Obukhv 1954; Stull 1988). The parameterization scheme used in this study is

summarized in Jacobson (2005) and is briefly described below.

The $K_{jj,atm}$ in the surface layer of the atmospheric boundary layer was calculated using Equation (3).

$$K_{atm} = \frac{\kappa u_* z}{\phi(z/L)} \tag{3}$$

where z is the height at which the atmospheric diffusivity is calculated, and u_* is the calculated surface friction velocity. The Von Karman constant (κ) was taken as 0.35. Parameter ϕ was used to account for the stability of the atmosphere and was calculated based on the Monin-Obukhov length (L), which in turn was calculated using Equation (4) and (5).

$$L = \frac{u_*^2 t_s}{\kappa g t_*} \tag{4}$$

$$t_* = \frac{\kappa(t_s(z_r) - t_s(z_{0,h}))}{\int_{z_{0,h}}^{z_r} \phi(z/L)\frac{dz}{z}} \tag{5}$$

where t_* and t_s are the potential temperature scale at the surface layer and the virtual temperature at the ground surface, respectively.

Equations (6), (7), and (8) were used to calculate the function ϕ in stable (L>0), unstable (L<0), and neutral (L=0) atmospheric conditions, respectively.

$$\phi\left(\frac{z}{L}\right) = 0.74 + 4.7z/L \tag{6}$$

$$\phi\left(\frac{z}{L}\right) = 0.74 + (1 - 9 \times z/L) \tag{7}$$

$$\phi\left(\frac{z}{L}\right)=0.74 \tag{8}$$

The $K_{jj,mw}$ needs to be evaluated before Equation (1) can be used to solve the reactive transport of pollutants. Bäumer et al. (2005) suggested using Equation (9) for the additional turbulent kinetic energy (e_m) caused by the moving vehicles.

$$\begin{aligned}\frac{\partial e_m}{\partial t} &= -\frac{\partial (Ue_m)}{\partial x}-\frac{\partial (Ve_m)}{\partial y}-\frac{\partial (We_m)}{\partial z} \\ &+\frac{\partial}{\partial x}\left(K_{xx}\frac{\partial e_m}{\partial x}\right)+\frac{\partial}{\partial y}\left(K_{yy}\frac{\partial e_m}{\partial y}\right)+\frac{\partial}{\partial z}\left(K_{zz}\frac{\partial e_m}{\partial z}\right)+P-\varepsilon\end{aligned} \tag{9}$$

In this equation, P and ε denote the rate of production and dissipation of kinetic energy, respectively, and K_{xx}, K_{yy}, and K_{zz} are turbulent diffusivities in the x, y, and z directions. The ability of vehicles to produce turbulence in the atmosphere is a function of their geometries and speeds. Detailed calculation of the vehicle-induced turbulence for every possible vehicle shape and speed combination is too complex to be implemented in a 3D air quality model and has to be parameterized. In the parameterization scheme, the vehicle fleet was divided into two general classes, passenger cars (pc) and heavy-duty vehicles (hd). The vehicles were represented by a representative height and width. The production of turbulent kinetic energy due to passenger cars and heavy-duty vehicles was calculated using Equation (10).

$$P=\frac{0.5}{L_x L_z}\left(c_{d,pc}W_{pc}H_{pc}T_{pc}V_{pc}^2+c_{d,hd}W_{hd}H_{hd}T_{hd}V_{hd}^2\right) \tag{10}$$

Here, L and c_d denote the grid length and drag coefficient, respectively. Mean width, mean height, travel velocity, and traffic density of a vehicle class are denoted by W, H, V, and T, respectively.

The energy dissipation at a height, z, above the surface was calculated using Equation (11).

$$\varepsilon=c_1\frac{e_m^{1.5}}{z} \tag{11}$$

The kinetic energy updated at each time step was used to calculate the coefficient of diffusion due to turbulence created by a moving vehicle using Equation (12).

$$K_{jj,mw} = \overline{L}_j \times e_m^{0.5} \tag{12}$$

where $\overline{L}_j$ is the length of a vehicle along axis *j* and can be calculated by Equations (13) and (14).

$$L_{xx} = \left(\frac{T_{pc} W_{pc} + T_{hd} W_{hd}}{T_{pc} + T_{hd}} \right) \tag{13}$$

$$L_{yy} = \left(\frac{T_{pc} H_{pc} + T_{hd} H_{hd}}{T_{pc} + T_{hd}} \right) \tag{14}$$

Gas Phase Chemical Mechanism

A modified version of the SAPRC99 (Carter 2000) photochemical mechanism was used to perform gas phase chemistry in the near-road environment. SAPRC99 is a lumped chemical mechanism used to study the photo-oxidation of organic compounds and inorganic compounds in the atmosphere and is widely used in regional air quality models. The original version was modified to explicitly include chemical reactions of some air toxics for vehicular emissions. An asymptotic technique presented in Young and Boris (1977) was used to solve the ordinary differential equations (ODEs) of chemical reactions involving 69 chemical species included in the model.

2.1.2. Solution Techniques for the Reactive Transport Equation

Operator Splitting Solution of the Governing Equation

The solution of the reactive transport equation followed the operator splitting procedure described by McRae et al. (1982). In this technique, different parts of the reactive transport equation are solved sequentially using the most suitable technique. For each operator splitting time step, Δt, the advective and diffusive transport of pollutants in the horizontal direction is solved using a time step of Δt/2. The 2D transport is performed by solving the one-dimensional (1D) transport equation in the x and y individually. In the first Δt/2 time step, the pollutant transport of species in the x direction is followed by the transport in the y

direction. After the horizontal transport, chemistry, emission, vertical diffusion, and dry deposition processes are solved together with a time step of Δt, followed by another horizontal transport calculation with a time step of Δt/2, with y direction first and then x direction, to complete an entire time step of the simulation. In the present study, the operating time step was 1 second (s). This choice was based on the wind speed in the domain and allowed for a stable solution of the transport equation.

Diffusion

The Crank-Nicholson method, as shown in Equation (15), was used to solve the diffusion of pollutants.

$$\frac{c_i^{n+1} - c_i^n}{\Delta t} = \frac{K}{2x^2}\left(\left[c_{i+1}^n - 2c_i^n + c_{i-1}^n\right] + \left[c_{i+1}^{n+1} - 2c_i^{n+1} + c_{i-1}^{n+1}\right]\right) \tag{15}$$

where n, x, and i denote the time step, grid length, and grid number, respectively. Equation (15) can be arranged in the form of a tri-diagonal matrix and was solved using a subroutine from the numerical recipe book (Press et al., 1992).

Advection

The piece-wise parabolic method (PPM) was used to solve the advection equation (Corlella and Woodward, 1984). The advantage of the PPM method is it allows non-uniform grid size in the model. In this procedure, a cubical curve fitting technique that is piece-wise continuous in nature is used to interpolate the concentration at each grid edge. The slope of the parabola at the edge of the grid, *j*, is given by Equation (16).

$$\delta C_j = \frac{\Delta e_j}{\Delta e_{j-1} + \Delta e_j + \Delta e_{j+1}}\left(\frac{2\Delta e_{j-1} + \Delta e_j}{\Delta e_{j-1} + \Delta e_j}\left[C_{j+1} - C_j\right] + \frac{2\Delta e_{j+1} + \Delta e_j}{\Delta e_{j-1} + \Delta e_j}\left[C_j - C_{j-1}\right]\right) \tag{16}$$

Here, Δe_j denotes the size of the grid, *j*.

The concentration at the next time step (C_j^{n+1}) was calculated using Equation (17).

$$C_j^{n+1} = C_j + d_j\left(fl_{j-1} - fl_j\right) \tag{17}$$

where d_j, a dimensionless number given by Equation (18), was plugged into Equation (19) to

calculate fl_j.

$$x_j = \frac{u_j \Delta t}{e_j} \tag{18}$$

$$fl_j = C_{rj} - \left(\frac{x_j}{2} \times \left[\left\{ C_{rj} - C_{lj} \right\} - \left\{ \left[1 - \frac{2x_j}{3} \right] \times C_{6,j} \right\} \right] \right) \tag{19}$$

Here, e, u, C_r, and C_l represent size, wind velocity, and concentration at the right and left boundary, respectively. $C_{6,j}$ is given by Equation (20).

$$C_{6,j} = 6(C_j^n - 0.5(C_{rj} + C_{lj})) \tag{20}$$

2.2. Modeling SF_6 Dispersion near a Simulated Freeway

2.2.1. GM Experiment

General Motors conducted experiments at its Milford Proving Ground in 1976 to study the exposure to sulfate near roadways. The study was done on 17 different days, from September 27 to October 30. The experiments were conducted on a simulated four-lane bidirectional freeway using 352 catalyst-equipped cars divided into 32 packs, with 16 packs of cars in each direction. The fleet also included eight pickup trucks equipped with cylinders releasing SF_6 at known rates to study dispersion near freeways. Each pickup truck was placed four packs apart. Figure 2 shows a section of the freeway with packs of cars.

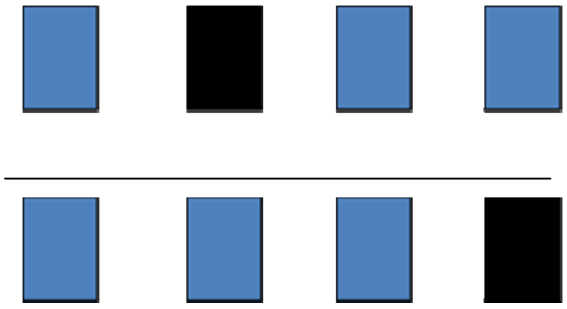

Figure 2. A section of the freeway showing packs of cars

NOTE: A pack of cars with a truck is represented with a different colored pattern.

The meteorological conditions and the concentration of sulfate and SF_6 were measured at six towers arranged in the upwind and downwind locations near the simulated freeway. Wind direction at the GM Proving Ground during the experiment was generally from west to east. Tower 1 and 2 were at 30 m and 2 m west of the freeway left boundary (in the upwind direction), respectively. Tower 3 was placed at the median of the freeway, which separated the northbound and southbound traffic. Towers 4–6 were arranged at 4, 15, and 30 m east of the freeway right boundary (downwind), respectively. In addition to these towers, two stands were placed at 50 and 100 m east of the freeway to measure concentrations and meteorological conditions at 0.5 and 1.5 m above the surface, respectively. All the towers and stands were placed in a straight line, as shown in Figure 3.

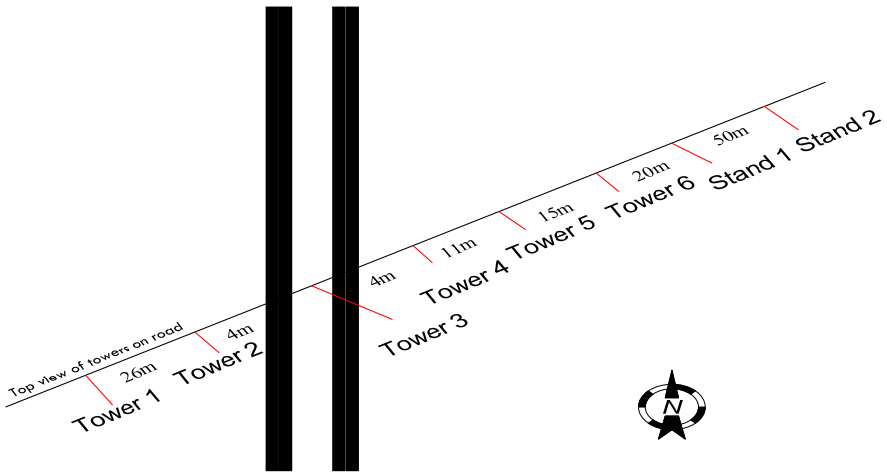

Figure 3. The alignment of six towers and two stands

The arrangement of the samplers and meteorological instruments on the towers can be seen in Figure 4. Temperature was measured at three different heights, 1.5, 4.5, and 10.5 m, on towers 1 and 6. UVW anemometers, used to measure wind speed in x, y, and z directions, were placed at three heights, 1.5, 4.5, and 10.5 m, on all the towers and at 1.5 m on the two stands. Syringe samplers were placed at 0.5, 3.5, and 9 m above the surface to collect SF_6 samples in all the towers and at 1.5 m height on the stands. The collected samples were analyzed using a gas chromatograph to determine the SF_6 concentration.

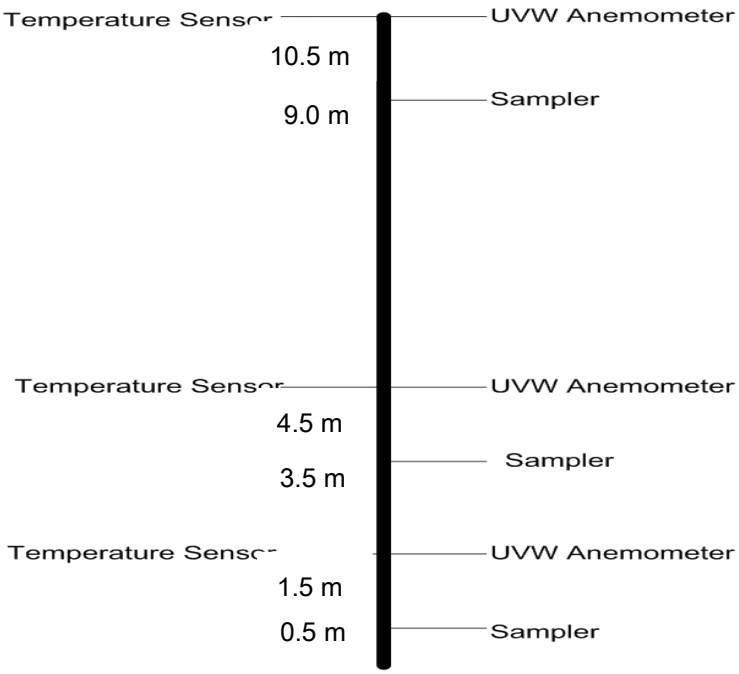

Figure 4. Schematic view of a tower

Sampling started at 7:35 AM and ended at 9:35 AM on most of the 17 study days. In this period, four half-hour samples were collected. Each sample was denoted by a specific number, "dddhhmmss," which will be referred to hereafter as a "scode." For example, scode 296083459 denotes the half-hour sample collected on the 296th Julian day of the year, from 8:04:59–8:34:59. A total of 66 SF_6 tracer data were collected during this study. However, not all the samples collected could be used for analysis. On day 272, leaks in the SF_6 tracer release system were observed. On days 272–276, thermometers used to collect temperature data at the 30 m west tower (tower 6) malfunctioned. As temperature was used in the calculation of atmospheric diffusivity, we excluded the data collected on these days from our calculations and thus ended up with 50 scodes for analysis.

2.2.2. Model Domain

The modeling domain in this study was a rectangular domain of 600 x 600 m in the horizontal direction and 40 m in the vertical direction. The domain was divided into 100*100*11 grids. Each grid cell was 6 x 6 meters in the horizontal direction**.** The four-lane north-south freeway was placed at 42, 48, 66, and 72 m from the left boundary of our domain. The model domain is shown in Figure 5. The vertical spacing of the grid cells varied from 1

m near the surface to 10 m in the top layer (i.e., the height of each layer is 1 m, 1 m, 2 m, 2 m, 2 m, 2 m, 4 m, 4 m, 6 m, 6 m, and 10 m, respectively, from bottom). A finer vertical spacing near the surface was taken to study the pollutant transport in detail in the lower regions of the atmosphere.

As the meteorology available from the GM experiment was only to a height of 10.5 m above the surface, a logarithmic wind profile was inserted in order to extrapolate the data to higher elevations in the domain.

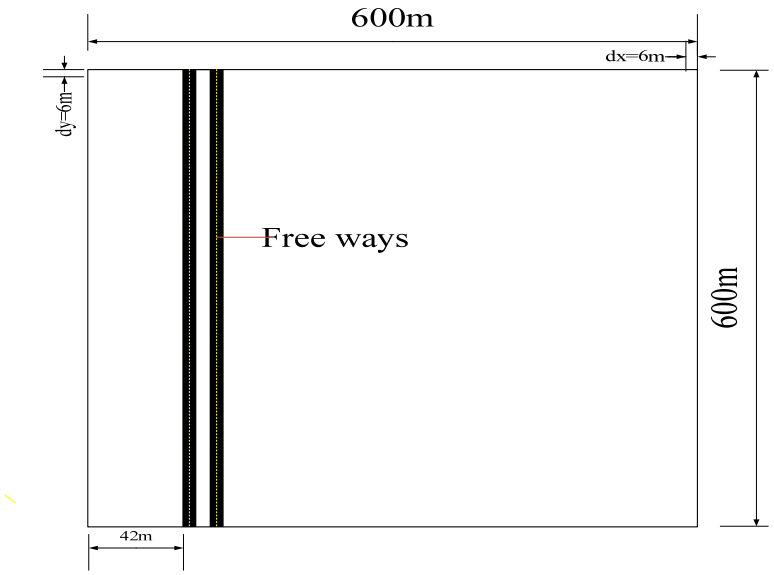

Figure 5. Model domain

2.2.3. Vehicle Density and Emission Rate of SF_6

The total amount of SF_6 emitted from all the trucks in a lane was averaged over all the grids in that lane. In other words, emission rates of SF_6 in l/min in each lane (f) were converted into ppm/s in each road grid (F) using Equation (21). Here, 8.4 e-7 is the conversion factor from l/min from a lane to ppm/s in a grid. For example, on Julian day 272, the flow rate was reported as 1.41 l/min from an inside lane and was calculated as 11.84 e-7 ppm/s per a grid.

$$F = f 8.4 \times 10^{-7} \tag{21}$$

The number of vehicles (N) in a freeway grid area (a) was calculated using the vehicle

density per unit area, as illustrated in Equation (22). The vehicle density was 0.003 vehicles/area, which is about 0.1(0.003*36) vehicles per grid.

$$N = n \times a \tag{22}$$

As there were no chief sources of SF_6 apart from the amount emitted from the cylinders placed in the trucks, the boundary concentration and the initial concentration of SF_6 were considered as 0.

2.2.4. Results

Determine the Parameters of Vehicle-Induced Turbulence

The parameterization used to calculate vehicle-induced turbulent diffusivity had two empirical constants: c_1 in the energy dissipation term (Equation [10]) and $c_{d,pc}$ in the kinetic energy production term (Equation [11]). Proper values for the two empirical constants, $c_{d,pc}$ and c_1, were determined through a series of model simulations with different $c_{d,pc}$ and c_1 combinations to minimize the sum of the squared residuals (SSR) between the prediction and observations using the entire GM dataset. The best values for $c_{d,pc}$ and c_1 are 0.4 and 8×10^{-3}, respectively.

Base Case Simulation Results

In order to understand the model performance with respect to the wind direction, the experiments were divided in three categories. Category A (225–315 degrees from north), Category B (315–337.5 and 202.5–225 degrees from north), and Category C (337.5–22.5 and 157.5–202.5 degrees from north) represent wind directions that are perpendicular, oblique, and parallel to the highway, respectively. Since the design of the GM experiment assumed a dominant westerly wind and only two samplers were placed to the west of the road, easterly wind cases were not included in the analysis.

Figure 6 shows the paired comparison of the observed and predicted SF_6 concentrations for 12 selected 30-minute sampling experiments. Four experiments were selected for each wind direction category. The total number of data points included in the figure is 240. The correlation coefficient (R), slope, and interception for a linear fit between predicted and observed concentrations is 0.812, 1.16 (±0.11, 95% confidence interval), and -0.168 (±0.12),

respectively. This suggests that the slope is statistically close to 1 and the intercept is close to 0. The data points were divided into three different groups based on the height where the observations were made. Most of the data points fall between the 2:1 and 1:2 lines, indicating a good model performance. The linear fit parameters with 95% confidence interval and the correlation coefficients are also shown in Figure 6. Highest concentrations generally occur at the surface, and the model slightly under-predicts these concentrations. The model performance appears to be best for the concentrations measured at 3.5 m above the surface. At 9 m above the surface, the model over-predicts the concentrations.

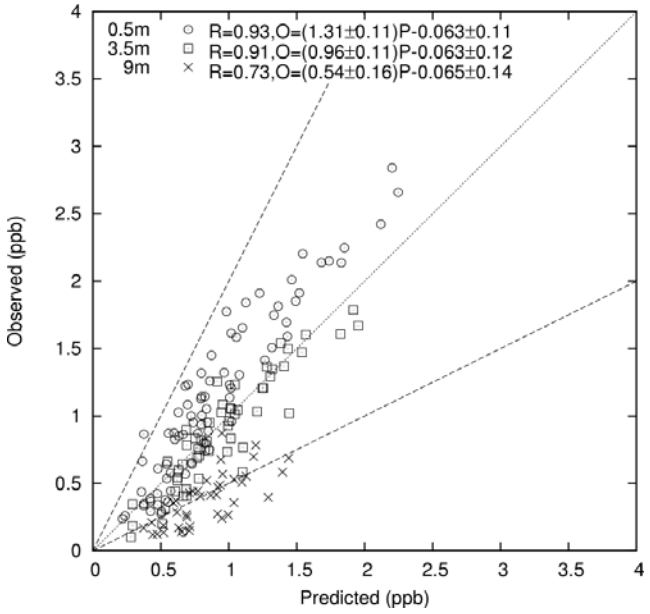

Figure 6. Predicted and observed concentrations of SF_6 for all the simulated cases

NOTE: The uncertainties shown in the slopes and intercepts reflect the 95% confidence interval of these values (O: observation, P: prediction).

The model performance was further evaluated using statistical measures of fractional bias (FB) and normalized mean square error (NMSE). Table 1 shows the comparison of the FB and NMSE from the TAMNROM-3D and ROADWAY-2 models, which also reported model performance with GM's SF_6 dataset. Both models slightly under-predicted the concentrations under perpendicular wind conditions with a similar model performance. TAMNROM-3D performed significantly better for oblique wind cases with a small over-prediction. Both models performed well under parallel wind conditions. Further analysis showed that 90% of the TAMNROM-3D predictions were within a factor of 2 of the observed concentrations, compared to 80% for the ROADWAY-2 model. Overall, TAMNROM-3D satisfactorily

reproduced the SF_6 experiments at all wind directions. A similar comparison with the UCD 2001 model indicated that the TAMNROM-3D performs similar to the UCD 2001 model, which performs better than the CALINE models (Held et al., 2003).

Table 1. FB and NMSE for TAMNROM-3D and ROADWAY-2

Wind Category	TAMNROM-3D		ROADWAY-2	
	FB	NMSE	FB	NMSE
Perpendicular (A)	-0.07	0.15	-0.11	0.30
Oblique (B)	0.05	0.15	-0.55	0.52
Parallel (C)	0.05	0.12	0.12	0.10
Overall	0.001	0.13	-0.18	0.29

Note: FB = $2(\overline{P}-\overline{O})/(\overline{O}+\overline{P})$, NMSE = $\overline{(P_i-O_i)^2}/(\overline{O}\times\overline{P})$, where $\overline{O}$ and $\overline{P}$ are mean observed and predicted concentrations.

The sum of squared residuals (SSR) and α, which denotes the percentage by which the predictions vary with observations, were calculated for the complete dataset using Equation (23) and (24), respectively, and they are shown in Table 2. According to Rao et al. (1986), an α value of 30 shows excellent model performance. Held et al. (2003) used the same GM data to analyze their model (UCD 2001) and the U.S. EPA's previously used regulatory models, CALINE3 and CALINE4. These evaluation results, adapted for comparison purposes in this study, are also presented in Table 2.

$$SSR = \sum_{i=1}^{n} \left(P_i - O_i\right)^2 \tag{23}$$

$$\alpha = \sqrt{\frac{SSR}{\sum_{i=1}^{n} P_i^2}} \tag{24}$$

Table 2. α and SSR for our model, UCD 2001, CALINE3, and CALINE4 (Held et al. 2003)

Model	α (in percent)	SSR	N_s
This study	50	544	50
UCD 2001	38	180	62
CALINE3	104	1353	62
CALINE4	92	1068	62

These results indicated that the performance of our model was comparable to UCD 2001, while it was better than the CALINE3 and CALINE4 models. As discussed earlier, a total of 12 scodes that had a problem with measured temperature were not analyzed by our model. The other models reported in the table above were less temperature dependent and so may have included those 12 scodes in their analysis.

Figure 7 shows the observed and predicted concentrations for the wind categories, perpendicular (A), oblique (B), and parallel (C), at three elevations above the surface along the downwind distance from the simulated highway. Error bars on each data point represent the standard deviation from the mean value. Averaged over all cases, the predicted peak SF_6 concentrations at 0.5 m were in the range of 1.2–1.5 ppb for the three wind categories. The observed concentrations were around 2–2.2 ppb. The difference between the prediction and observation decreased at downwind locations. At 3.5 m, the model predictions agreed well with the observations at all locations. The observed spatial gradients of SF_6 were also well reproduced. Both predictions and observations showed that highest concentrations occurred when the wind was parallel to the highway. The panels on the third row show that the model over-predicted the concentrations at 9 m above the surface. Errors in the predicted diffusivity fields or wind fields were the likely causes for this over-prediction.

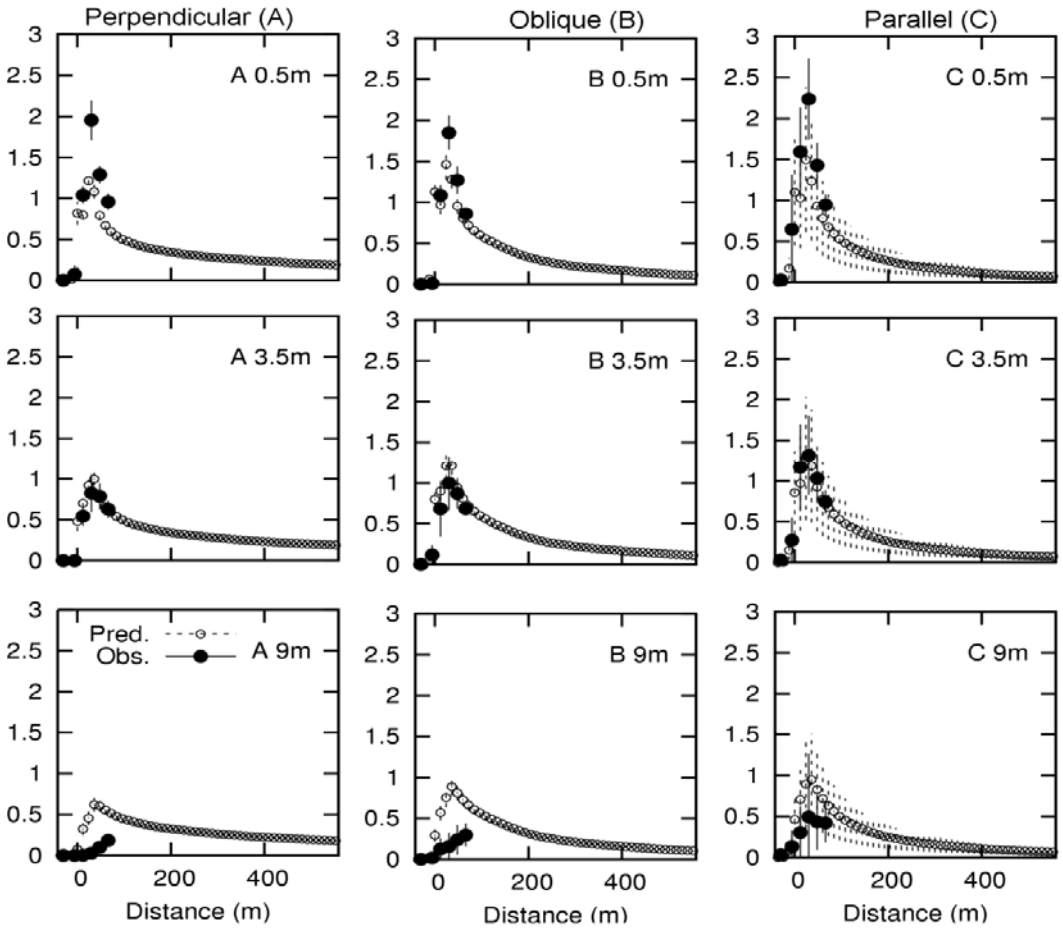

Figure 7. Observed and predicted spatial distribution of SF_6 concentrations (ppb)

Figure 8 illustrates the importance of the vehicle induced turbulence (VIT) parameterization in predicting pollutant concentrations in a near-road environment. Open circles show the comparison of the base case predictions with observations, as shown in Figure 6. The filled circles are the predicted SF_6 concentrations when the VIT is not included in the dispersion calculation, i.e., only advection and diffusion due to atmospheric turbulence were included. Without VIT, the concentrations were significantly over- and under-predicted. A close look at the model results shows that surface concentrations were significantly over-predicted while concentrations at 3.5 and 9 m were generally under-predicted.

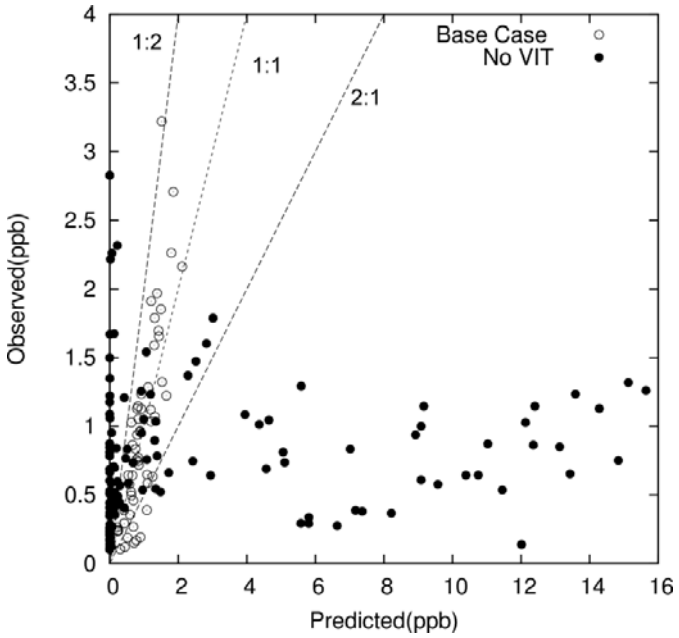

Figure 8. Predicted SF_6 concentrations compared with observations

2.2.5. Sensitivity Analysis

Meteorology Inputs

Advections by the mean wind and turbulent diffusion are two important processes that determine the pollutant dispersion. Measured wind speed by wind sensors is associated with uncertainty. This uncertainty is introduced using the average wind for the domain and vertical interpolation. The atmospheric turbulent diffusivities, calculated using the measured wind shear and temperature profiles, also have significant uncertainty. The magnitude of the uncertainty in predicted SF_6 concentrations to the uncertainty in wind field and calculated diffusivity was studied using a Monte-Carlo simulation technique.

One hundred simulations were conducted for a representative case in each wind category using randomly generated wind speeds and diffusivities that followed a normal distribution curve with a standard deviation of 30% around the original wind speed and diffusivity. Although wind speed and turbulent diffusivity are not independent, they were treated as independent variables in this analysis. The mean values and standard deviations for the predicted SF_6 concentrations at monitor locations were determined from the 100 simulations and were compared to observations in Figure 9(a). While the error bars on predictions represent 1 standard deviation (σ) from the mean value, the error bars on observations

indicate a measurement accuracy of 3% (1σ), as reported in Cadle et al. (1976). A 30% uncertainty in the meteorology led to uncertainties of 0.1–0.2 ppb in most cases. The magnitude of the uncertainty appeared to not be correlated with the absolute value of the predicted concentration. The mean concentrations from the Monte-Carlo simulation were also compared with the base case predictions and showed excellent agreement. No deviation was noticed. Based on this analysis, we concluded that the uncertainties in the meteorology inputs did not lead to significant biases in the model results.

Vehicle Drag Coefficient and TKE Dissipation Rate

The vehicle drag coefficient and turbulence kinetic energy (TKE) dissipation rate directly affect the intensity of TKE created by moving vehicles and thus indirectly affect the overall turbulent diffusivity and the pollutant concentrations. In order to better understand the sensitivity of the predicted concentrations to the selection of the vehicle drag coefficient ($c_{d,\,pc}$) and the proportionality constant (c_1), another set of Monte-Carlo simulations was conducted by assuming an uncertainty of 50% for both parameters.

Similar to the meteorology inputs study, 100 simulations were conducted for a representative case in each wind category using randomly generated positive values for $c_{d,pc}$ and c_1 that followed a normal distribution curve with a standard deviation of 50% around the original $c_{d,pc}$ and c_1 values of 0.4 and 8×10^{-3}, respectively. As c_1 and $c_{d,pc}$ cannot be negative, 2.3% of the hundred random numbers generated were removed from the analysis. The mean values and standard deviations for the predicted SF_6 concentrations at monitored locations were determined from the 100 simulations and were compared with the observations in Figure 9(b). Unlike meteorology inputs, the predicted uncertainties due to statistically independent $c_{d,pc}$ and c_1 appeared to correlate with the mean predictions. The relative uncertainty in the predictions varied from 5–20%, with most cases in the 10–15% range. The uncertainties in the c_1 and $c_{d,pc}$ more effectively affected the concentrations near the surface but not significantly at 9.5 m above the surface. Again, the predicted mean values of the SF_6 concentrations from the Monte-Carlo simulations were compared with the base case predictions, and no deviation was detected. In conclusion, the predicted SF_6 concentrations did not change significantly with reasonable variation in the $c_{d,pc}$ and c_1 values.

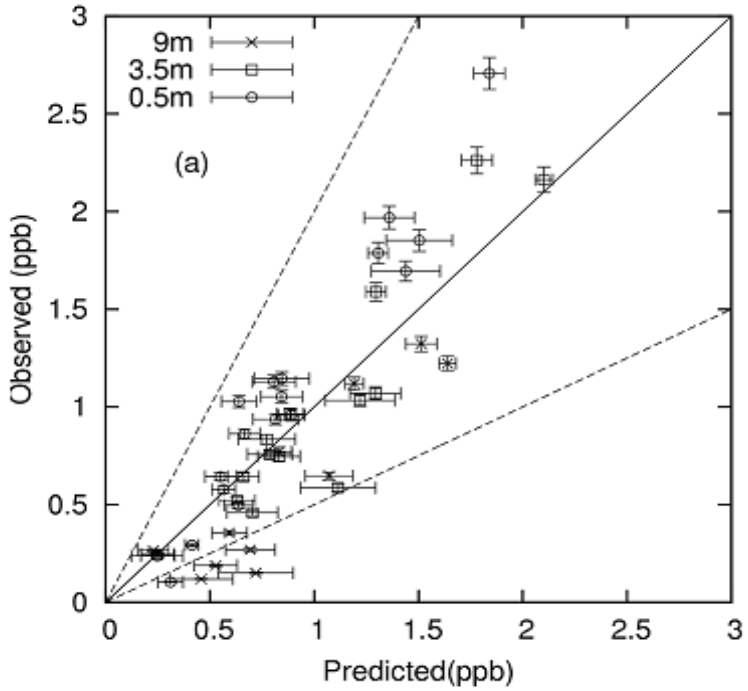

(a) 30% uncertainties in the wind speed and atmospheric turbulent diffusivity

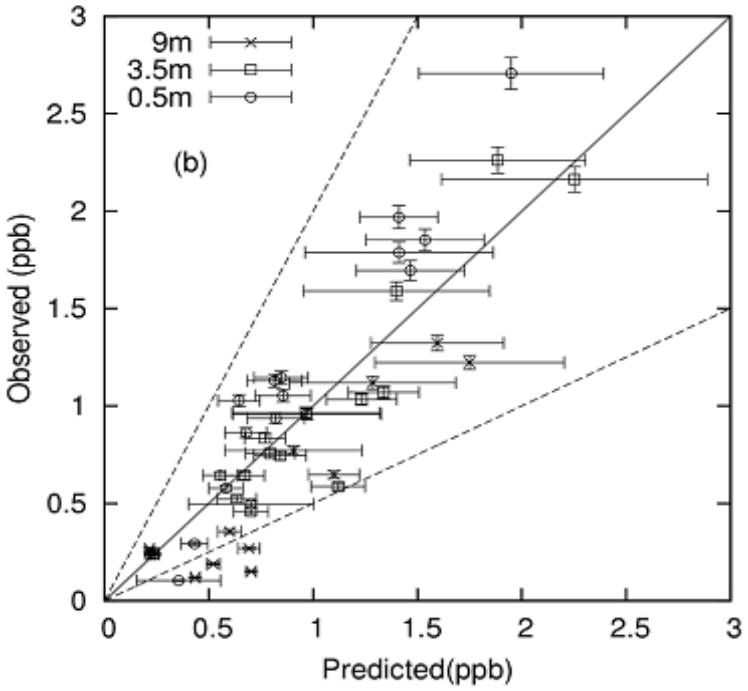

(b) 50% uncertainties in the model parameters $c_{d,pc}$ and c_1

Figure 9. Uncertainty of the predicted SF_6 concentrations

An additional simulation using the default $c_{d,pc}$ and c_1 values of 0.3 and 0.1, as reported by

Bäumer et al. (2005), led to slightly worse model performance. The correlation coefficient (R), slope, and interception were 0.76, 1.59, and -0.27, respectively. This suggested that the proper $c_{d,pc}$ and c_1 values were likely dependent on aerodynamic properties of vehicles and also meteorology conditions. The lower $c_{d,pc}$ value reported by Bäumer et al. might be due to less aerodynamic drag of vehicles made in the 1990s than vehicles made in the 1970s. Although $c_{d,pc}$ can be estimated with relative high confidence, more near-road datasets need to be analyzed in future studies to better estimate c_1 under various meteorology conditions. In absence of observation data to fit the two parameters, the default values can still be used as a first-order estimate.

Vehicle Speed and Density

Another source of uncertainty in predicting the pollutant concentrations is the variability in the vehicle speed and density that are used to estimate emission rates and to predict the turbulent diffusivity. Figure 10(a) shows the change in predictions when the vehicle density in each grid cell was doubled or halved, keeping the vehicle speed and SF_6 emission rate at each grid cell constant. The peak concentrations changed by only approximately ±20%, indicating that the model was less sensitive to the vehicle density alone. Figure 10(b) shows the sensitivity of the model to vehicle speed, when the vehicle density and the emission rate of SF_6 remain constant. It can be seen from the figure that doubling the vehicle speed by a factor of 2 leads to a reduction of the peak concentrations by approximately 50% compared to the base case. Similarly, a decrease in vehicle speed by 50% increases the peak concentrations by approximately a factor of 2. As expected, the model is more sensitive to the vehicle speed than the vehicle density because the TKE production is linearly proportional to the vehicle density but proportional to vehicle speed cubed.

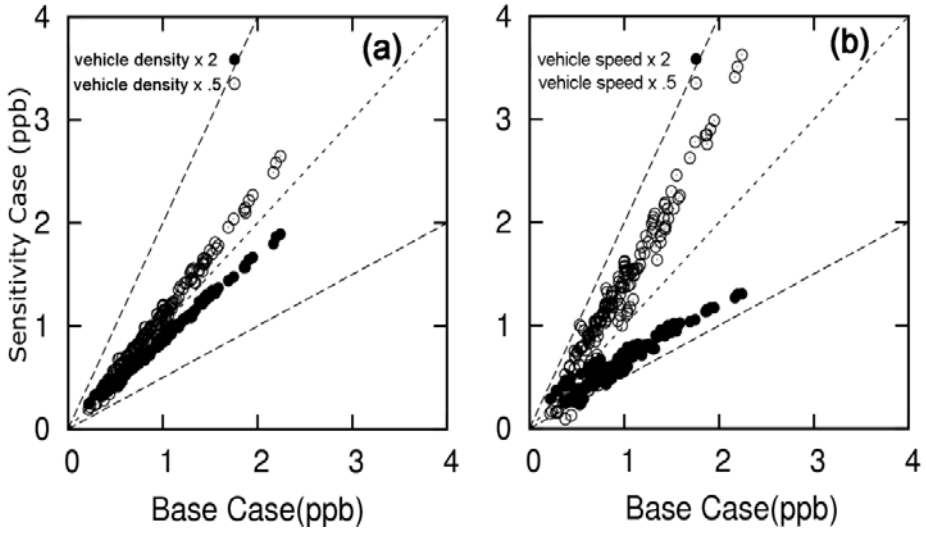

Figure 10. Sensitivity of the predicted SF_6 concentrations to the change in vehicle density and speed

Vertical Grid Resolution

In Eulerian models, space is discretized into a finite number of grid cells. Generally, higher grid resolution will lead to more accurate predictions. However, higher resolution simulations are slower and require more computation resources. The sensitivity of the predicted concentrations to the vertical grid resolution was studied by using a finer vertical grid setup. The number of vertical layers was increased from 11 to 30. The first 20 layers had a resolution of 1 m, and the remaining 10 layers had a resolution of 2 m. Figure 11 shows the predicted vertical profiles of SF_6 concentrations averaged using all the data points at tower 4. The results from the coarse grid were slightly lower than the fine-resolution results when the wind was parallel (category A) or oblique (category B) to the highway, with differences less than 5%. The fine-resolution results agreed very closely with the low-resolution results for parallel cases (category C).

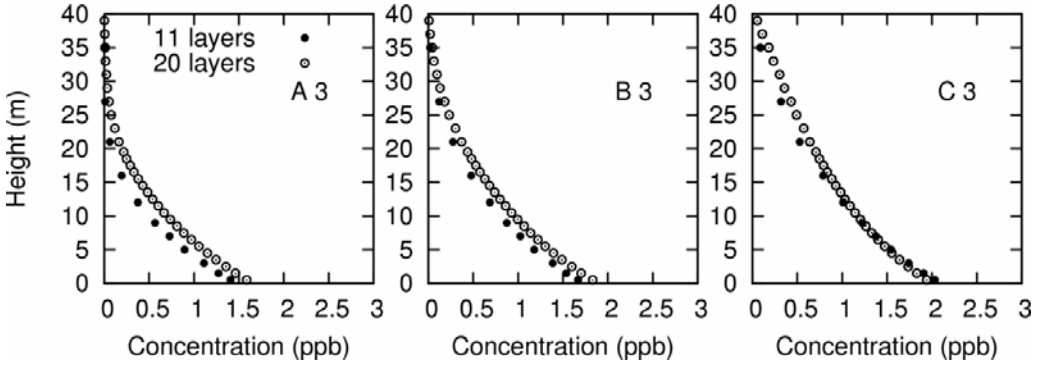

Figure 11. Comparison of the vertical SF_6 concentration profiles at tower 4 predicted by the base case model and the model with finer vertical resolution

2.3. Gas Phase Chemistry Simulations

2.3.1. Reactive Air Pollutants

A unique feature of the model developed in this study is that it incorporates the SAPRC99 gas phase atmospheric chemistry mechanism (Carter, 2000) that can be used to predict the formation and transformation of reactive air pollutants in a near-road environment. As reviewed in Section 1.2, most near-road air quality models are dispersion models and do not have a chemistry module. This limits their application in predicting only non-reactive chemical species. In this section, the importance of incorporated chemistry is studied in detail.

The important chemical reactions, which help in better interpretation of the results, were adapted from Seinfeld and Pandis (2006). The basic daytime photochemical reaction cycle is illustrated in Figure 12 and the relative equations are listed below (Equations [25]–[36]).

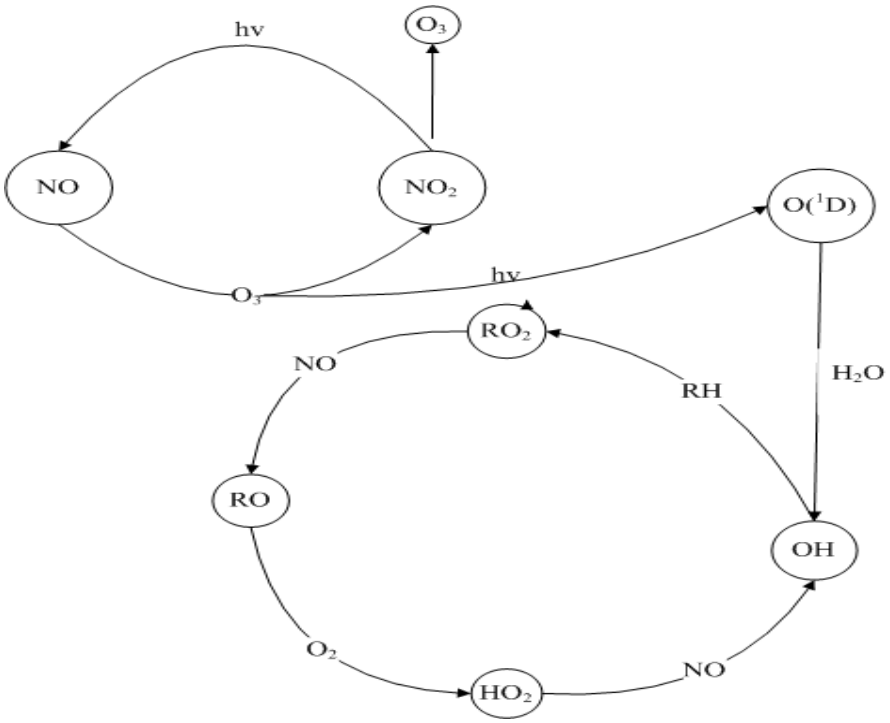

Figure 12. Basic daytime photochemical reaction cycle of NO, NO_2, radicals, and ozone in troposphere

$$NO_2 + h\nu \rightarrow NO + O \tag{25}$$

$$O + O_2 + M \rightarrow O_3 + M \tag{26}$$

$$O_3 + NO \rightarrow NO_2 + O_2 \tag{27}$$

$$O_3 + h\nu \rightarrow O_2 + O\left(^1D\right) \tag{28}$$

$$O\left(^1D\right) + H_2O \rightarrow 2OH^{\cdot} \tag{29}$$

$$RH + OH^{\cdot} \xrightarrow{O_2} RO_2^{\cdot} + H_2O \tag{30}$$

$$RO_2^{\cdot} + NO \rightarrow NO_2 + RO^{\cdot} \tag{31}$$

$$RO^{\cdot} + O_2 \rightarrow R'O_2 + HO_2 \tag{32}$$

$$HO_2^{\cdot} + NO \rightarrow NO_2 + OH^{\cdot} \quad (33)$$

$$HO^{\cdot} + HO^{\cdot} \rightarrow H_2O + O_2 \quad (34)$$

$$HO^{\cdot} + HO_2^{\cdot} \rightarrow H_2O + O \quad (35)$$

$$HO_2^{\cdot} + HO_2^{\cdot} \rightarrow H_2O_2 + O_2 \quad (36)$$

The emissions of NO_x and VOC from diesel- and gasoline-powered vehicles differ significantly. To better represent a busy freeway with both passenger and commercial traffic, it was necessary to use a reasonable split of gasoline and diesel vehicles in the fleet. Field studies conducted near freeways reported that diesel-powered vehicles represent about 20–30% of the total vehicle fleet (Zhu et al., 2002; Ntziachristos et al., 2007). The vehicle fleet in the base case of the present study was assumed to consist of 30% diesel-powered and 70% gasoline-powered engines.

To understand the effect of gas phase chemistry on the spatial distribution of air pollutants near freeways, eight different simulations were conducted. The base case simulation replicated a mid-afternoon scenario with a constant wind field blowing perpendicular to the freeway, selected from the GM study. The wind speed was approximately 1.3 m/s at 9.5 m above the surface, and the temperature was approximately 32°C. The upwind concentrations of pollutants were taken from a grid cell near downtown Houston using a regional air quality model simulation. The ozone concentration in the grid cell at noontime was quite low, approximately 30 ppb. This low concentration of ozone was likely due to the titration reaction of the ozone with the large amount of NO_x in the urban area. A different boundary condition that represented a grid cell in an ozone-rich plume downwind of the urban emission area was used in one of the case studies. A list of boundary species and their concentrations for the high-ozone and low-ozone scenarios are listed in Table 3.

Table 3. Concentration of boundary species for Case 1 (base case) and Case 5 (with high ozone boundary condition)

Species	Case 5	Case 1	Species	Case 5	Case 1
NO2	3.791099	35.12449	TBU_O	1.04E-08	3.34E-09
NO	0.332056	25.22054	ACET	2.869435	0.8624
O3P	1.54E-06	4.16E-06	NPHE	5.85E-02	2.57E-02
O3	141.2446	21.99543	PHEN	1.03E-03	3.64E-02
NO3	1.33E-03	4.91E-05	BZNO2_O	2.06E-06	3.61E-09
N2O5	1.04E-03	5.17E-04	HOCOO	4.02E-06	6.16E-09
HNO3	7.459017	4.299823	HCOOH	0.958399	9.38E-02
O1D2	6.90E-12	1.05E-12	RCHO	2.877141	1.005137
HO	5.30E-04	8.05E-05	GLY	0.162339	5.95E-02
HONO	1.75E-02	0.198843	MGLY	0.463394	9.37E-02
HO2	5.69E-02	2.69E-04	BACL	3.44E-02	1.17E-02
CO	210.6542	627.6038	CRES	1.26E-02	5.08E-02
HNO4	3.52E-02	1.93E-03	BALD	2.69E-02	4.43E-02
HO2H	2.077348	8.26E-02	METHACRO	0.210254	0.13192
SO2	17.12872	16.63903	MVK	0.648773	0.132364
SULF	1.13E-02	2.88E-03	ISOPROD	0.110603	8.80E-02
C_O2	2.02E-02	3.78E-05	DCB1	5.03E-02	0.12693
HCHO	10.9278	3.090503	DCB2	4.20E-03	6.39E-03
COOH	0.465848	5.70E-02	DCB3	1.36E-03	1.88E-03
MEOH	2.854117	1.097395	ETHENE	1.245501	4.387082
RO2_R	1.95E-02	1.01E-04	ISOPRENE	0.108218	0.123703
ROOH	1.537259	5.73E-02	TRP1	1.39E-03	2.59E-02
R2O2	4.78E-03	2.98E-05	ALK1	1.197291	2.992554
RO2_N	1.29E-03	9.53E-06	ALK2	1.209846	2.859279
RNO3	1.805857	0.487815	ALK3	2.836475	5.161239
MEK	3.317068	0.361934	ALK4	0.916839	4.732314
PROD2	1.803908	0.492026	ALK5	0.397094	3.25075
CCO_O2	6.28E-03	8.94E-06	ARO1	0.315296	2.007579
PAN	3.382097	7.52E-02	ARO2	0.125331	1.109794
CCO_OOH	0.417676	1.06E-02	OLE1	0.109478	1.544092
CCO_OH	0.797944	0.10623	OLE2	3.16E-02	0.734916
RCO_O2	2.75E-03	2.97E-06	PBZN	1.60E-02	1.38E-03
PAN2	2.150446	3.81E-02	BZ_O	3.06E-06	1.17E-07
CCHO	4.7612	1.506851	MA_RCO3	4.18E-04	6.29E-07
RCO_OOH	0.238483	3.92E-03	MA_PAN	0.420335	1.03E-02
RCO_OH	1.556649	0.141431	BZCO_O2	1.42E-05	7.84E-08

The major differences in the two cases were the abundance of primary emitted compounds. For example, the family of lumped alkanes, aromatics, and olefins was present at high levels in Case 1, and a higher concentration of photochemical oxidation products such as peroxy acetyl nitrate (PAN) were present in Case 5. This indicates that Case 1 represents a region in

an urban area with fresh emissions and Case 5 depicts a region farther from the urban area where higher concentrations of products are observed.

2.3.2. Modeling Emissions from Vehicles

The emission rates of gas phase pollutants from eight different vehicle types were prepared using MOBILE6, the EPA's mobile source vehicle emission factor model. MOBILE6 predicts the emission rates of NO_x, CO, VOC, and six air toxics, namely benzene (BENZ), methyl tertiary butyl ether (MTBE), BUTA, formaldehyde (HCHO), acetaldehyde (ACET), and acrolein (ACRO), in g/mi for 27 different vehicle types. The air quality model requires emissions in g/s for each grid cell, and the photochemical mechanism requires the predicted total VOC concentrations to be split into detailed VOC species. The air toxics are also explicitly tracked in the photochemical mechanism.

The emission factor (EF) in each grid was calculated using Equation (37).

$$EF = EM.\left(VS / 3600\right) \tag{37}$$

where EF is emission factor of a species in g/s at a freeway grid, EM is the raw emission factor in g/mi, and VS is average travel speed of all vehicle types considered in mi/hr. Emissions of the 27 different vehicle types predicted by the MOBILE6 were lumped into eight more general vehicle types. Table 4 shows the emission factors of different species in g/s for eight different vehicle types, light-duty gasoline (LDG), heavy-duty gasoline (HDG), motorcycle (MC), light-duty diesel truck (LDD), heavy-duty diesel vehicle (HDD), gasoline bus (GB), diesel commercial bus (DCB), and diesel school bus (DSB). Although only two vehicle types were used to split the vehicle fleet in our current study, this higher resolution of vehicle types allows the model to be applied to scenarios when detailed vehicle fleet information is available.

Table 4. Emission factors (g/s) of different model species for different vehicle types for a vehicle velocity of 60 mph

Species	LDG	HDG	MC	LDD	HDD	GB	DCB	DSB
NO	3.98E-04	4.90E-04	2.35E-03	1.00E-03	1.25E-03	8.77E-03	3.56E-04	6.91E-03
NO2	2.09E-05	2.58E-05	1.24E-04	5.28E-05	6.56E-05	4.61E-04	1.87E-05	3.64E-04
CO	1.26E-02	1.54E-02	3.51E-02	4.80E-04	6.09E-04	2.53E-03	1.18E-02	2.43E-02
SO2	1.80E-05	2.49E-05	4.74E-05	2.41E-05	3.36E-05	8.33E-05	8.57E-06	1.01E-04
NH3	9.67E-05	8.57E-05	4.42E-05	6.67E-06	6.67E-06	2.65E-05	1.11E-05	3.12E-05
BENZ	4.94E-06	6.56E-06	5.87E-06	1.46E-06	2.40E-06	1.64E-06	7.27E-06	5.50E-06
MTBE	2.81E-06	4.25E-06	3.97E-06	0.00E+00	0.00E+00	0.00E+00	5.50E-06	9.18E-06
BUTA	9.49E-07	1.65E-06	2.32E-06	9.47E-07	1.56E-06	1.38E-06	5.63E-06	2.41E-06
FORM	4.40E-06	1.04E-05	2.39E-05	7.31E-06	1.20E-05	3.18E-05	2.75E-05	3.48E-05
ACET	1.54E-06	3.01E-06	4.53E-06	1.59E-06	2.61E-06	7.98E-06	6.63E-06	7.69E-06
ACRO	9.03E-08	1.60E-07	1.40E-06	3.55E-07	5.84E-07	7.62E-07	3.12E-07	1.43E-06
ALK1	5.40E-06	8.85E-06	5.66E-06	0.00E+00	0.00E+00	0.00E+00	1.35E-05	0.00E+00
ALK2	4.81E-06	7.88E-06	2.52E-05	0.00E+00	0.00E+00	0.00E+00	1.21E-05	0.00E+00
ALK3	2.24E-05	3.68E-05	1.10E-04	0.00E+00	0.00E+00	0.00E+00	5.63E-05	0.00E+00
ALK4	2.54E-05	4.17E-05	8.53E-05	0.00E+00	0.00E+00	0.00E+00	6.38E-05	0.00E+00
ALK5	1.33E-05	2.18E-05	1.36E-05	0.00E+00	0.00E+00	0.00E+00	3.34E-05	0.00E+00
ARO1	9.39E-06	1.54E-05	1.32E-05	0.00E+00	0.00E+00	0.00E+00	2.35E-05	0.00E+00
ARO2	1.41E-05	2.30E-05	1.47E-05	0.00E+00	0.00E+00	0.00E+00	3.53E-05	0.00E+00
CCHO	7.37E-07	1.21E-06	0.00E+00	3.75E-06	6.17E-06	8.06E-06	1.85E-06	2.00E-05
CH4	7.24E-05	1.19E-04	3.77E-05	2.05E-05	3.38E-05	4.41E-05	1.82E-04	1.09E-04
ETHENE	1.61E-05	2.64E-05	3.83E-05	3.97E-05	6.53E-05	8.52E-05	4.04E-05	2.11E-04
HCHO	2.86E-06	4.68E-06	0.00E+00	1.63E-05	2.68E-05	3.50E-05	7.17E-06	8.68E-05
IPROD	3.31E-08	5.42E-08	0.00E+00	8.19E-07	1.35E-06	1.76E-06	8.30E-08	4.36E-06
ISOPRENE	1.19E-07	1.95E-07	3.62E-07	0.00E+00	0.00E+00	0.00E+00	2.99E-07	0.00E+00
MACR	1.24E-07	2.03E-07	0.00E+00	0.00E+00	0.00E+00	0.00E+00	3.11E-07	0.00E+00
NR	1.14E-05	1.87E-05	1.55E-05	2.96E-05	4.87E-05	6.35E-05	2.87E-05	1.58E-04
OLE1	5.85E-06	9.59E-06	2.09E-05	0.00E+00	0.00E+00	0.00E+00	1.47E-05	0.00E+00
OLE2	1.11E-05	1.81E-05	2.19E-05	0.00E+00	0.00E+00	0.00E+00	2.78E-05	0.00E+00
RCHO	3.99E-08	6.54E-08	0.00E+00	1.78E-06	2.92E-06	3.81E-06	1.00E-07	9.47E-06

The total emission rate of a species in a grid cell was calculated by Equation (38).

$$E_i = \sum_{j=1}^{M} EF_{i,j} \cdot N_j \tag{38}$$

where *i* is the species index, *j* is the vehicle type index, EF is the emission factor for a species predicted by Equation (37), M is the number of vehicle types, and N is the vehicle density of vehicle type *j* in a grid cell, given by Equation (39).

$$N_j = \left(\frac{V_j}{VS_j} \right).X_x \tag{39}$$

where V_j denotes the number of vehicles of type *j* travelling in a lane per hour, VS_j denotes the travel speed of vehicle *j* in m/hr, and X_x denotes the length of the grid at which the vehicle density is calculated.

The speciation profiles used to split the overall VOC into detailed SAPRC-99 VOC species are summarized in Table 5. Here, PC denotes a gasoline-driven passenger car, HD-gasoline indicates a gasoline-driven heavy-duty vehicle, and HD-diesel shows a diesel-driven heavy-duty vehicle.

Table 5. Speciation of VOCs from diesel- and gasoline-engine exhaust

Species	PC	HD-gasoline	HD-diesel
ALK1	0.000466	0.000229	0
ALK2	0.000415	0.001022	0
ALK3	0.001936	0.004473	0
ALK4	0.002193	0.003455	0
ALK5	0.001148	0.00055	0
ARO1	0.000809	0.000536	0
ARO2	0.001213	0.000595	0
CCHO	6.36E-05	0	0.000661
CH4	0.006241	0.001527	0.003616
ETHENE	0.00139	0.001551	0.006984
HCHO	0.000246	0	0.002867
IPROD	2.85E-06	0	0.000144
ISOPRENE	1.03E-05	1.47E-05	0
MACR	1.07E-05	0	0
OLE1	0.000505	0.000846	0
OLE2	0.000955	0.000888	0
RCHO	3.44E-06	0	0.000313

2.3.3. Discussions

Spatial distribution of ozone, nitrogen oxides, 1,3-butadiene (used to represent air toxics), carbon monoxide (as a non-reactive tracer), hydroxyl, and hydroperoxy radicals were predicted. In all these simulations, constant vehicle density and speeds were maintained. The details of the eight simulations are listed in Table 6.

Table 6. List of case studies conducted in gas phase simulation

Case	Comments
1	**Base Case**
2	**Similar to Case 1, chemistry disabled**
3	**Similar to Case 1, with wind parallel to the freeway**
4	**Similar to Case 1, with parallel wind, chemistry disabled**
5	**With higher boundary ozone concentrations (approximately 140 ppb)**
6	**Similar to Case 5, chemistry disabled**
7	**Similar to Case 1, with higher diesel fraction in vehicle fleet, i.e., 50% gasoline-powered and 50% diesel-powered vehicles**
8	**Similar to Case 7, chemistry disabled**

In all the simulations other than the cases when the wind was parallel to the freeway, it took less than 10 simulated minutes for the model to reach a steady state in the entire domain. The change of the ozone concentration as a function of time at 6, 36, and 438 m away from the highway is show in Figure 13. From the figure, it can be seen that the time for the ozone to reach a steady state was 50, 125, and 300 seconds at the three different distances. The parallel cases took a longer time to reach a steady state because the horizontal dispersion in the direction perpendicular to the freeway was mainly due to turbulent diffusion, which is comparatively slower than advection. This suggests that to better simulate the air quality near the freeway when the wind is near parallel, transient simulation is probably needed. The concentration predicted using steady-state assumption may not correctly reproduce the air quality a few hundred meters away from the freeway.

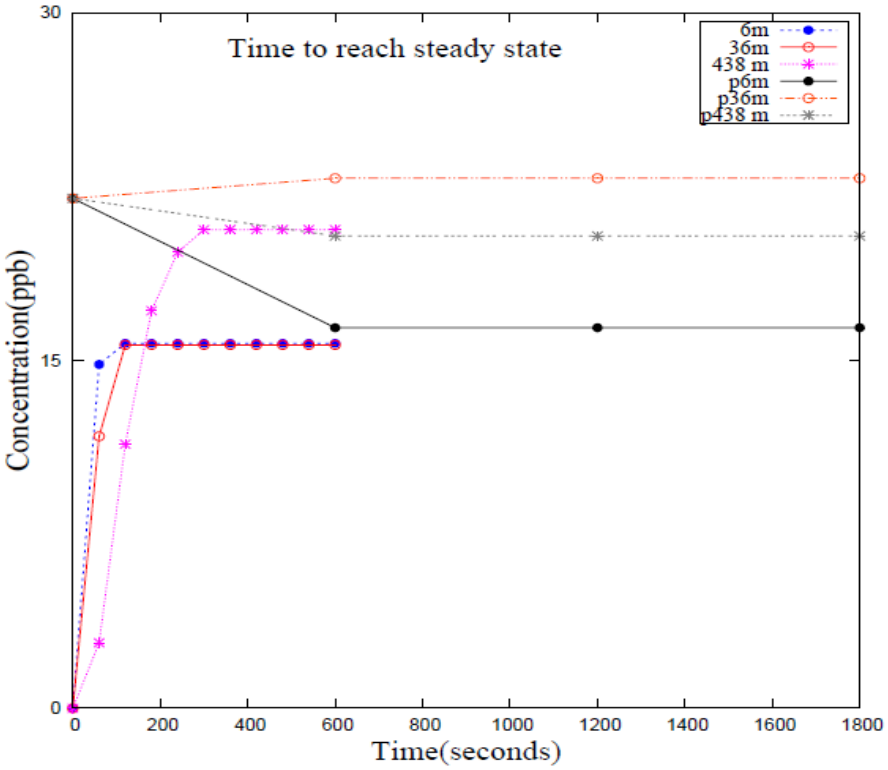

Figure 13. Change in ozone concentration with time at the heights of 6, 36, and 438 m

NOTE: From the right boundary of the freeway in Case 1(base case) and Case 3 (with wind parallel to freeway and denoted by *p* in the figure)

Base Case Simulation

Figure 14 depicts the results of two different simulations, with a chemical mechanism included in one (Case 1) and excluded in another (Case 2). From the figure, it is clear that there is a slight change in the concentrations of the species due to incorporating chemistry to the model. Changes observed in each of these species are explained below.

A clear decrease in the ozone concentrations near the simulated freeway was predicted when the gas phase chemistry was enabled. Without gas phase chemistry, only a slight decrease in concentration was observed, likely caused by the dry deposition of the ozone during the transport process. The decrease in the ozone concentrations near the freeway may be chiefly attributed to the reaction of ozone with high concentrations of NO near a freeway due to emission from vehicle traffic, as explained in reaction Equation (27). In addition, ozone photolysis may have also partly contributed to this decrease. The observed gradual rise in ozone concentration away from the freeway was chiefly due to a decrease in NO

concentration, which led to the formation of NO_2, as shown in reaction Equation (27). As the distance away from the freeway increased, the concentration of NO decreased, resulting in a decrease in ozone concentrations lost due to reaction Equation (27).

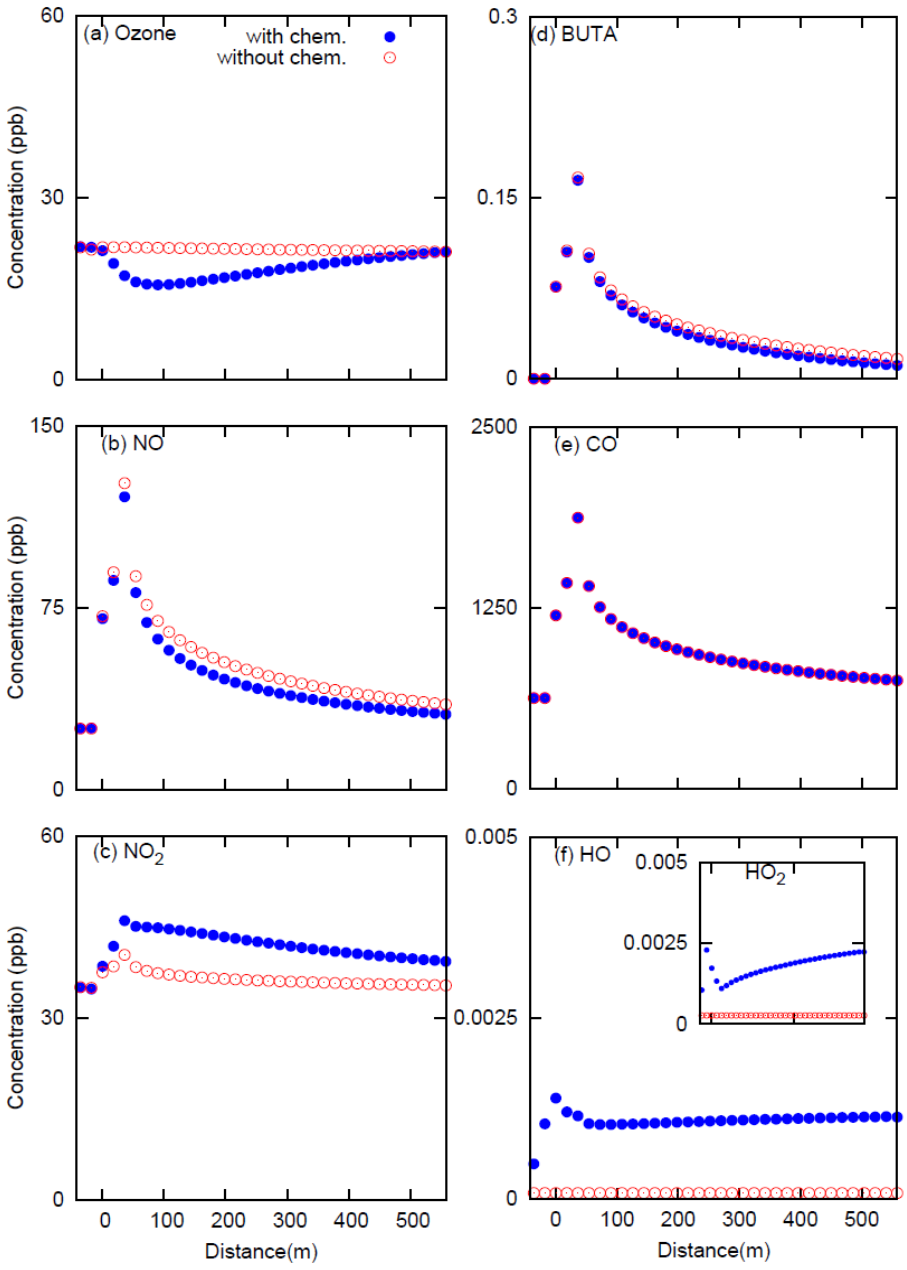

Figure 14. Concentrations of different pollutions with and without chemistry at noontime

NOTE: A positive x-axis indicates downwind distance from the starting point of the freeway.

The sharp rise in nitric oxide concentrations near the simulated freeway, as seen in Figure 14(a), was chiefly due to the emission of NO from vehicles. Comparatively lower

concentrations in Case 1 (with gas phase chemistry) than in Case 2 (without chemistry) were due to the reaction of NO with ozone that led to the formation of nitrogen dioxide in Case 1, as explained in reaction Equation (27).

In Figure 14(c), it can be seen that NO_2 concentrations near the freeway were comparatively higher in Case 1 than in Case 2. This was mainly due to the formation of NO_2 from the reaction of NO with ozone, as explained in reaction Equation (27). In both cases, NO_2 changed more slowly with distance from the freeway than NO. This higher dilution was due to a higher difference in concentration of NO produced near a freeway when compared to background concentration.

In addition to NO_x and O_3, it is also interesting to look at the spatial distribution of less reactive species, CO and BUTA, near the freeway. CO is less reactive than BUTA and is often used as a tracer for vehicle emissions. BUTA is considered a hazardous air pollutant (HAP) that could increase human cancer risk. It was selected in this study because its reaction with oxidants in the air are faster and it has greater cancer risk than many other air toxics (Darnall et al., 1976) and even has greater cancer risk (Seiber, 1996; Morrow, 2001). These characteristics make it a better candidate to study the effect of chemistry on the spatial distribution of air toxics. As seen in Figure 14(d) and (e), there was a rapid increase in CO and BUTA concentrations at the freeway, and concentrations started to fall with the distance away from the freeway in both cases. There was little change in the concentrations predicted from Case 2 due to a relatively low hydroxyl radical concentration, which makes the lifetime of BUTA near a freeway relatively long.

A hydroxyl radical (HO) is formed in the environment due to the reaction of a water vapor molecule with an excited oxygen atom $O(^1D)$, as shown in reaction Equation (27). In the troposphere, $O(^1D)$ is mainly produced by the photolysis of ozone. Figure 14(f) shows that a slight increase in the HO concentration at the freeway from the boundary concentration of 0.483 ppt to 1.14 ppt HO_2 decreased, while OH increased in this case. The relative distribution of HO and HO_2 is generally governed by the VOC/NO ratio.

Concentration Profiles at Different Heights

Figure 15 shows the concentration profiles of the species at different elevations in the domain. As discussed in the previous chapter, the domain was divided into 11 layers, with finer

resolution grid cells near the surface to better resolve pollutant gradients. The concentrations of each model species at the boundary of the domain at each layer were the same as they were in the surface layer. The concentration profiles of the seven species at five layers, 1, 3, 6, 9, and 11 (the center of the layers were 0.5, 3, 9, 21, and 35 m above surface, respectively), are shown in Figure 15.

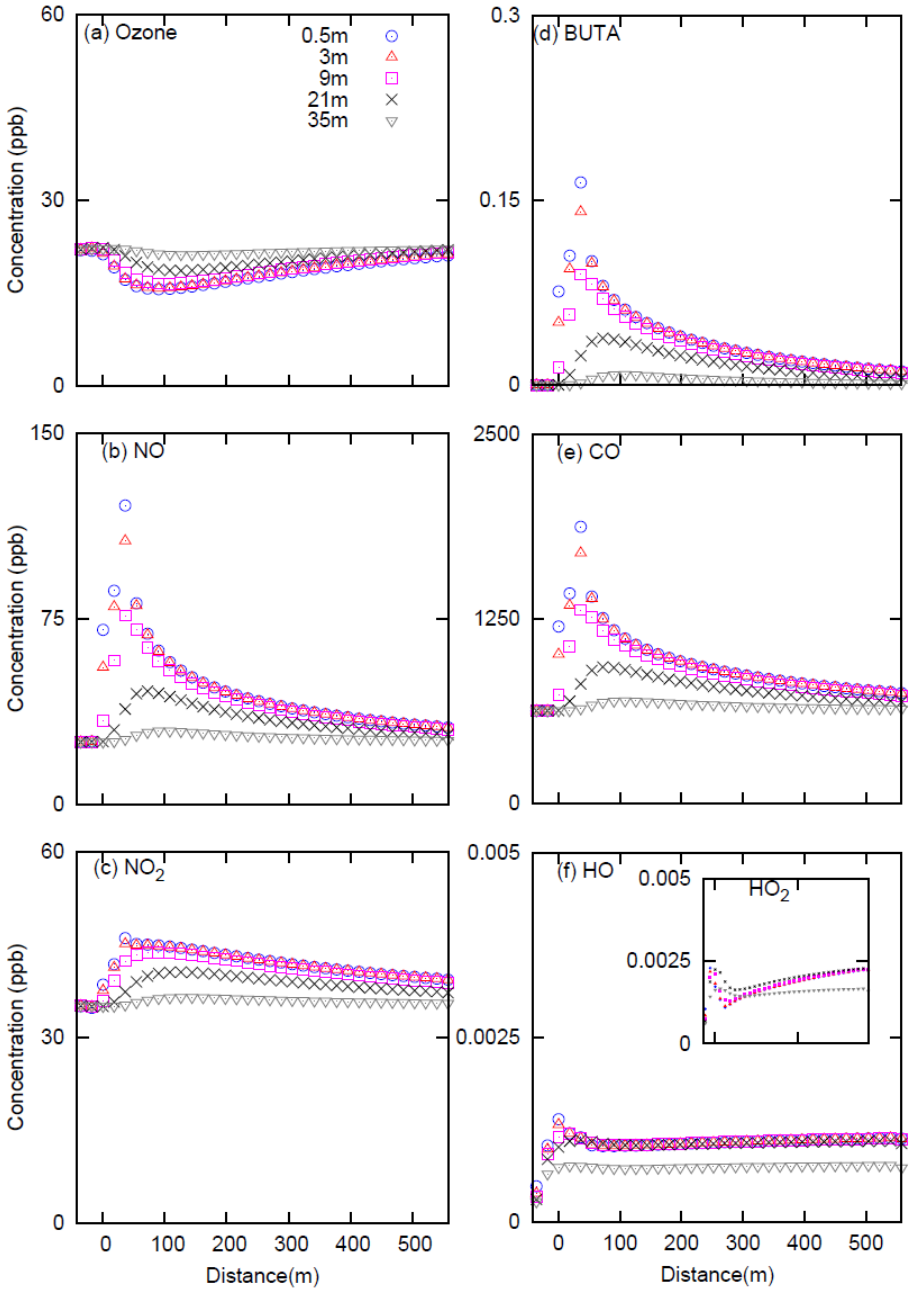

Figure 15. Concentration profiles at different heights in the model domain for Case 1

In Figure 15(a), a rise in concentration of ozone at the freeway with height in the domain is observed. As explained in reaction Equation (27), reaction of ozone with nitric oxide is one of the chief contributors to the removal of ozone in a near-road environment, so the rise in ozone concentrations was due to the fall in NO concentrations at different layers, as seen in Figure 15(b). The concentrations of NO, NO_2, CO, and BUTA decreased with height in the domain. The fall in peak concentrations near the freeway indicated the lesser concentrations of these species that undergo a vertical transport from the surface layer where they were emitted.

In Figure 15(f), a fall in concentration of HO and a rise in HO_2 concentration with an increase in height in the domain are seen. This fall in peak concentrations of HO can be coupled to a relative decrease in NO concentrations when compared to a decrease in VOC concentrations with an increase in height.

Wind Blows Parallel to the Freeway

Figure 16 shows the importance of chemistry when the wind blows parallel to the freeway. In these cases, the initial concentration of species at all the layers was set to their respective boundary concentrations. Thus, the time of simulation in this case was reduced by adapting a uniform concentration throughout the domain, as it reduced the time taken for the species emitted from the freeway to diffuse to other regions in the model domain. Results of two different simulations, Case 3 (with chemistry) and Case 4 (without chemistry), are shown in the figure. The results of the base case simulation are also presented in the figure for comparison purposes.

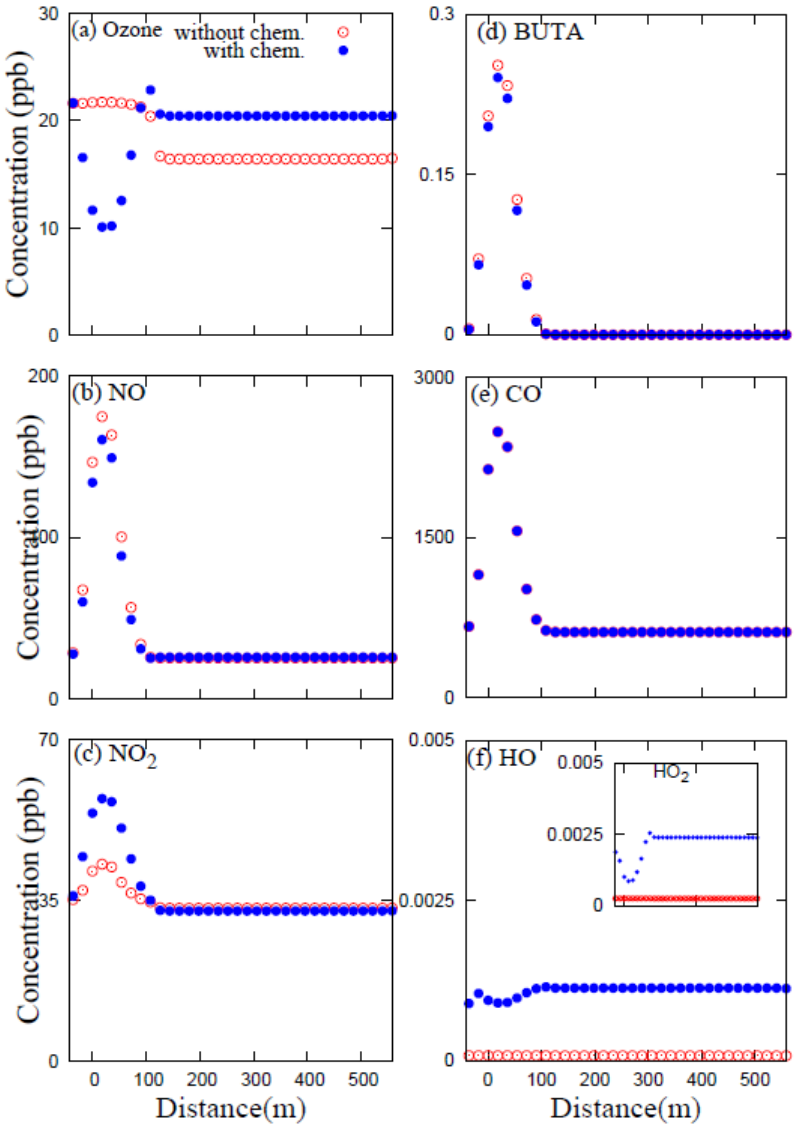

Figure 16. Concentration profiles with and without chemistry at the surface layer

When comparing Figure 16 (wind parallel to freeway) and Figure 14 (wind perpendicular to freeway), a higher concentration of species (NO_x, CO, and BUTA) emitted from vehicles at the freeway but lower concentrations of the same in the areas adjacent to the freeway are observed in cases with wind parallel to the freeway. For example, peak concentrations of NO, NO_2, CO, and BUTA predicted at the freeway in Case 4 (without chemistry) were approximately 101, 82, 12, and 67% higher, respectively, than concentrations predicted in Case 2 (base case, without chemistry). This difference was attributed to higher concentrations of pollutant advecting in the direction of the freeway when the wind was parallel to the freeway. The observed change in concentration profiles of the species in Figure 16 are explained below.

A higher fall in concentration of ozone is observed in Figure 16(a) (Case 3, with chemistry), when compared to the fall observed in Figure 14(a) (Case 1, with chemistry). This pattern was chiefly attributed to the higher concentration profile of NO near the freeway, observed in Figure 16(b), as the concentration of ozone lost due to reaction with NO to form NO_2, as explained in reaction Equation (27), varied with the concentration of NO.

In Figure 16(b), a higher peak concentration of NO at the freeway in Case 4 (without chemistry), when compared to Case 3 (with chemistry), is observed, depicting the absence of reaction of NO with ozone to form NO_2.

Figure 16(c) shows that at the freeway, the peak concentration of NO_2 in Case 3 (with chemistry) is about 35% higher than the peak concentration observed in Case 4 (without chemistry). This is higher than the difference (about 14%) of NO_2 in Figure 14(c). This difference in relative concentration is due to the higher concentration of NO depicted in Figure 16, which leads to NO_2 formation, as explained in reaction Equation (27).

In the Figure 16(f), a higher concentration of radicals, both HO and HO_2, in Case 3 (with chemistry) is predicted, when compared to Case 4 (without chemistry), which have an almost uniform concentration of 0.08 ppt and 0.26 ppt, respectively, and similar to boundary concentration throughout the domain. A higher fall of HO_2 at the freeway in the subplot of Figure 16(f), when compared to the fall in Figure 14(f), is observed. This higher fall can be explained by the fall in the observed VOC/NO ratio.

High Ozone Boundary Condition Simulation

Figure 17 shows the spatial distribution of species in the regions where higher ozone boundary concentrations are observed. Results of simulation for two different cases, Case 5 (with chemistry) and Case 6 (without chemistry), are shown.

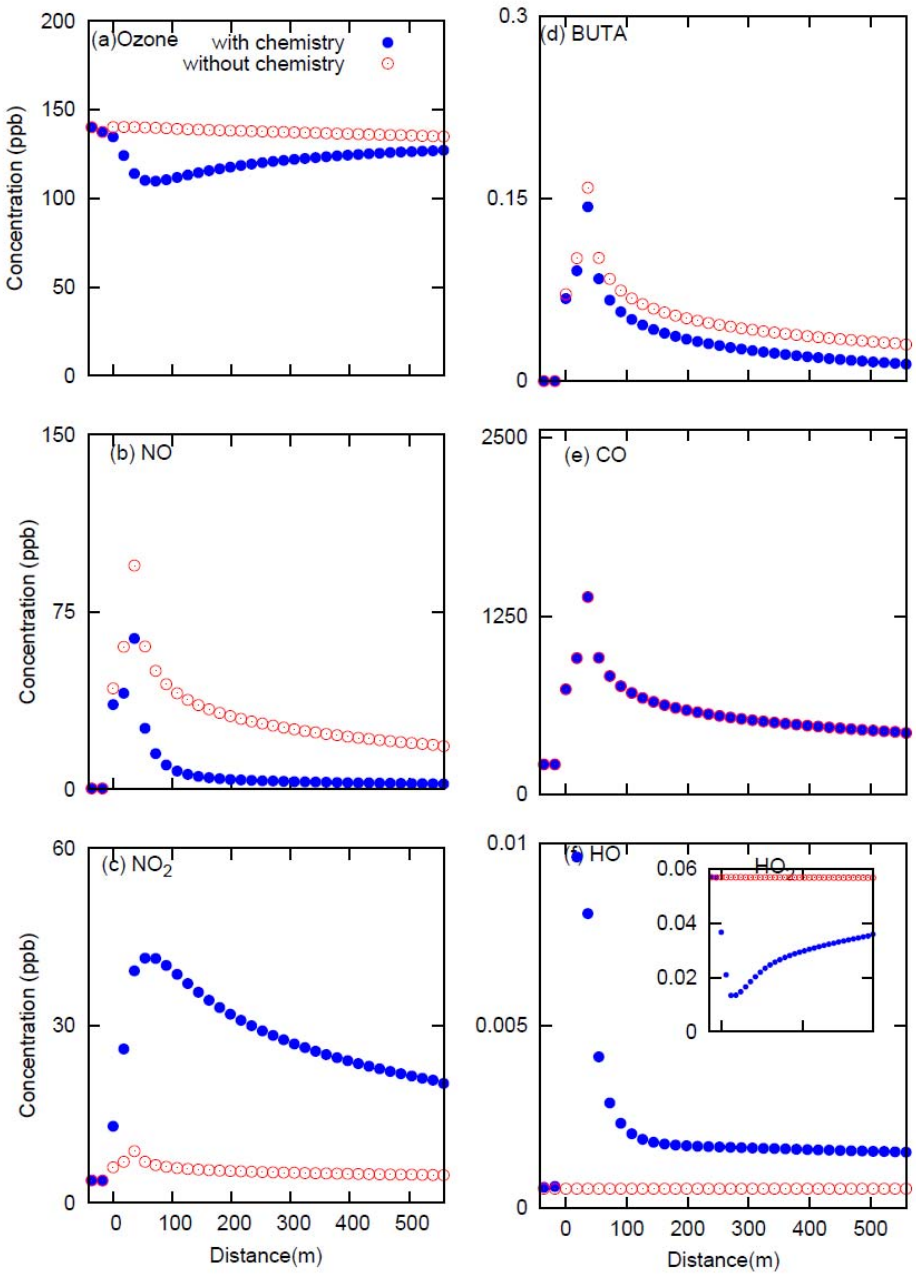

Figure 17. Concentrations of different pollutions with higher boundary concentrations of ozone (Cases 5 and 6)

The concentration profiles of each species observed in Figure 17 are discussed below.

In Figure 14(b) and Figure 17(b), a greater fall in peak NO concentrations in Case 5 (with chemistry, higher boundary ozone) than in Case 1 (with chemistry, base case boundary ozone), compared to their corresponding cases, Case 6 and Case 2, is seen. This higher difference can be attributed to higher ozone concentrations in Case 6 and Case 5, which

instigate the formation of NO_2 from NO, as shown in reaction Equation (27). Similarly, a greater rise of about 300% in the concentration of NO_2 at the freeway in Case 5 (with chemistry) is illustrated in Figure 17(c), compared to a rise of about 13% in Case 1 (base case, with chemistry), as seen in Figure 14(c). This change can be attributed to higher ozone concentrations, which lead to a higher depletion of NO and a higher formation of NO_2, as explained by reaction Equation (27).

An interesting scenario is observed in Figure 17(f). A higher difference in the concentration of the HO_2 radical is observed at the freeway in Case 5 (with chemistry) when compared to Case 6 (without chemistry), compared to the difference observed in the subplot of Figure 14(f). The boundary concentration of HO_2 also increased by a factor of 10, when compared to Case 1 (base case, with chemistry). This increase in boundary concentration can be explained by higher ozone and higher VOC/NO ratio in the boundary of the domain, as explained later in Figure 19.

Similarly, a higher rise in concentration of HO is observed in Figure 17(f) (approximately 7.5 ppt), compared to Figure 14(f) (approximately 0.9 ppt). This can be attributed to a relative rise in NO concentrations when compared to the rise in VOC near a freeway, as seen later in Figure 19. It is also interesting to see a higher concentration range for HO_2 compared to HO throughout the domain, when compared to Case 1 (base case) or Case 7 (with higher diesel fraction), where almost similar concentration ranges are observed. This higher range of HO_2 is due to higher VOC/NO ratio when compared to the base case.

Higher concentration of HO radicals in Case 5 (with chemistry), when compared to concentrations predicted in Case 1 (base case, with chemistry) lead to a higher difference (about 11%) in peak concentrations of BUTA, as seen in Figure 17(d), in cases with and without chemistry, when compared to just 1% difference seen in Figure 14(d) (base case).

Higher Diesel Fraction

Figure 18 shows the concentration profiles of species when the fleet comprises a higher fraction of diesel-powered vehicles. The simulation results of Case 7 (with chemistry) and Case 8 (without chemistry) are shown in this figure.

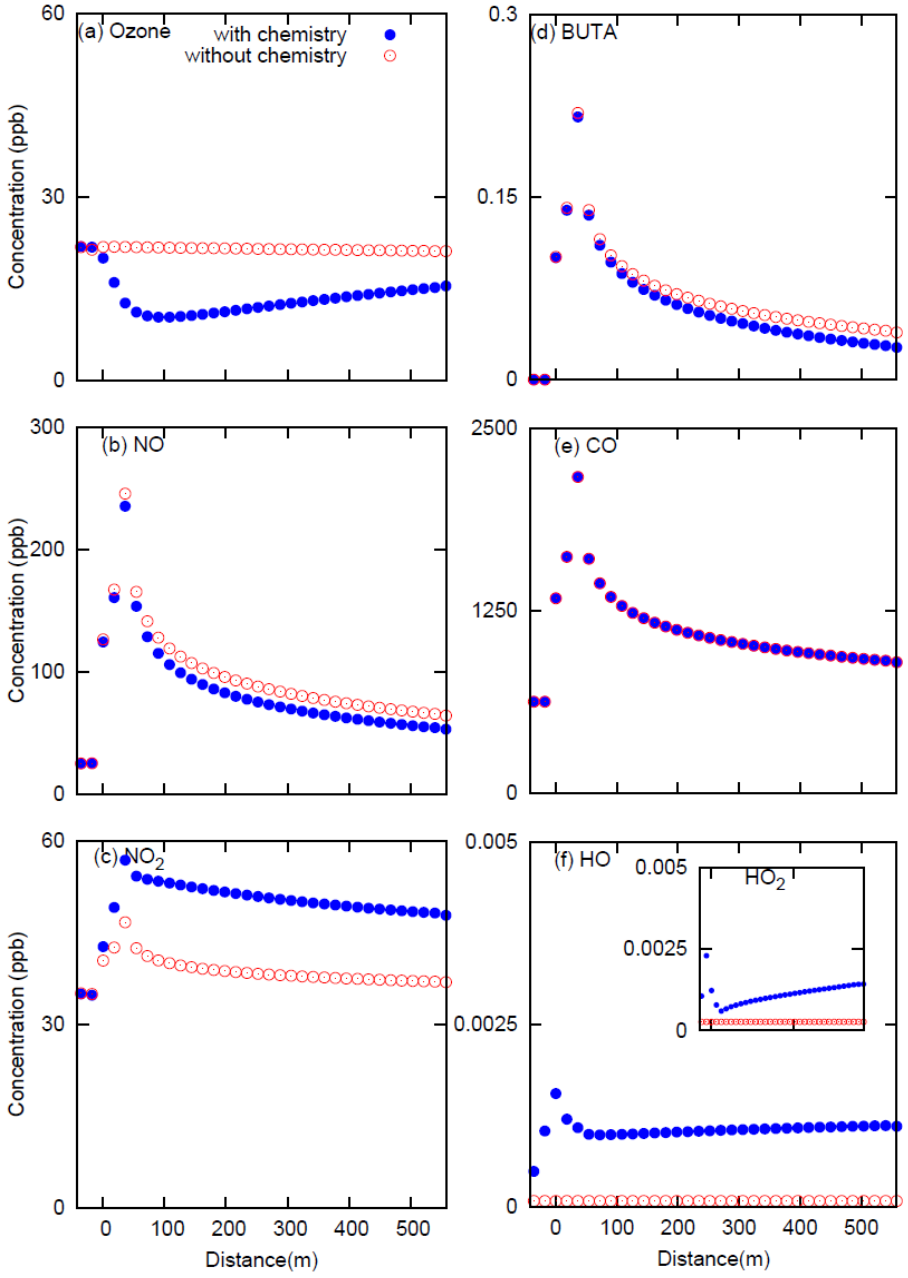

Figure 18. Concentrations of different pollutions with higher diesel fraction in vehicle fleet (Cases 7 and 8)

As diesel vehicles produce more NO_x than gasoline vehicles, the peak concentrations of NO_x observed in Case 7 and 8 are higher than those of the base cases (Case 1 and 2). For example, peak concentrations of NO and NO_2 in Case 8 (without chemistry) were about 94% and 15% higher than their corresponding peak concentrations predicted in Case 2 (base case, without chemistry). A higher increase in NO_2 observed in Case 7 (with chemistry, higher diesel

fraction), as seen in Figure 18, when compared to the rise in Case 1 (with chemistry, base case) seen in Figure 14 was due to higher concentrations of NO, as explained in reaction Equation (27).

In Figure 14(a) and Figure 18(a), a greater fall in concentration of ozone is predicted in the case with higher diesel fraction (Case 7, with chemistry) than in Case 1 (base case, with chemistry). This extra fall can be attributed to the higher NO concentration in Case 7 and 8, when compared to their corresponding base cases (Case 1 and 2), because the removal mechanism of ozone is its reaction with NO, as explained in reaction Equation (27).

A slight increase in HO concentrations and a slight decrease in HO_2 concentrations in Case 7 (with chemistry) are seen in Figure 18(f). This change is due to the lower VOC/NO ratio observed in Case 7 (with chemistry, high diesel), when compared to Case 1 (with chemistry, base case).

An increase in concentration peaks of CO and BUTA by about 15% and 30%, respectively, in Case 8 (without chemistry), when compared to Case 2 (base case, without chemistry), is observed. This rise can be attributed to the increase in diesel-powered engines in the vehicle fleet. A slightly higher fall in BUTA in cases where chemistry is included in Figure 18(d), when compared to Case 1 (with chemistry, base case) in Figure 14(d), is due to slightly higher OH concentrations observed in Figure 18(f), when compared to those in Figure 14(f).

Factors Affecting HO and HO_2 Concentration

Levy (1971) used reaction Equations (25)–(36) and showed that in a normal atmosphere, the steady state relation between HO_2 and OH can be given by Equation (40), (41), and (42).

$$\frac{\left[HO_2^{\cdot}\right]}{\left[HO^{\cdot}\right]} = \frac{k_{OH^{\cdot}-RH}[RH]}{k_{HO_2^{\cdot}-NO}\left[NO\right]} \tag{40}$$

$$\left[HO_2^{\cdot} + HO^{\cdot}\right] = \sqrt{\frac{2k_{O(^1D)-H_2O}\left[O(^1D)\right]\left[H_2O\right]}{k_{OH-OH}}} \tag{41}$$

$$\left[HO^{\cdot}\right] = \left(\frac{\sqrt{\frac{2k_{O(^1D)-H_2O}\left[O(^1D)\right]\left[H_2O\right]}{k_{OH-OH}}}}{1+\frac{k_{OH^{\cdot}-RH}[RH]}{k_{HO_2-NO}\left[NO\right]}} \right) \tag{42}$$

From Equation (40), we observe that in a system at steady state, the ratio of HO_2 to OH chiefly depends on the ratio of VOC to NO, i.e., an increase in VOC/NO results in an increase in HO_2/HO and vice versa. From Equation (41), it can be seen that the overall HO_x concentration is proportional to the $O(^1D)$ concentration; thus, it is proportional to ozone concentration. Equation (42) can be derived by combining Equation (40) and (41). It can be seen that two factors affect the HO_x concentration, ozone concentration, and VOC/NO ratio. HO concentration is proportional to the ozone concentration and inversely proportional to the VOC/NO ratio. Depending on the ratios of the hydrocarbon-hydroxyl oxide (RH-HO) reaction rate and the NO-HO_2 rate, the effect of the VOC/NO ratio on HO concentration can vary.

Figure 19 shows the ratio of VOC and NO throughout the domain for Case 1 (base case), Case 3 (with wind parallel to freeway), Case 5 (with higher ozone boundary concentration) and Case 7 (with higher diesel fraction in vehicle fleet).

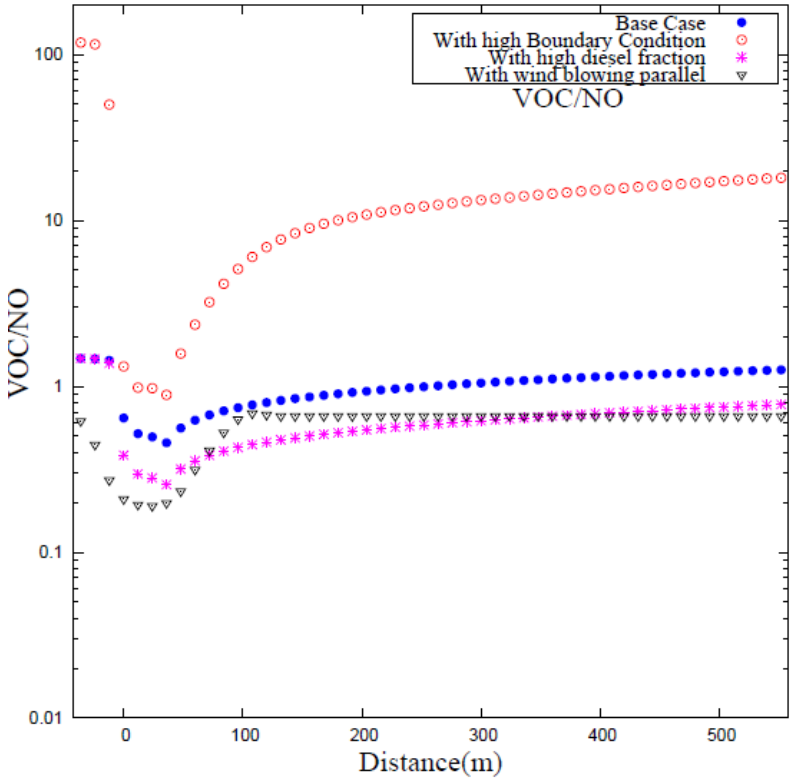

Figure 19. VOC to NO ratio for four different cases: Cases 1, 3, 5, and 7

NOTE: "0" on the X-axis indicates the starting point of the freeway.

In Figure 19, a fall in VOC to NO at the freeway region (i.e., 0 to 36 m on X-axis) is observed in all the cases. This shows the relative higher concentration of NO when compared to VOC emitted from a vehicle exhaust. The decrease in the VOC/NO ratio qualitatively explained the increase in the HO concentration. The VOC/NO ratio for Case 5 (with higher ozone boundary condition) was slightly higher than Case 1 (base case), and this could be attributed to higher ozone and lower NO being available at the boundary. A lower VOC/NO is observed in Case 7 (with higher diesel fraction) when compared to Case 1 (base case). This was attributed to the increase in diesel fraction in the vehicle fleet, which emitted high NO when compared to a gasoline vehicle. The high ozone concentration explained why the highest HO concentration occurs in Case 5 near the freeway. The significant HO decrease in that case was well predicted by the sharp decrease in the VOC/NO ratio.

3. MODELING TRAFFIC ASSIGNMENTS WITH AIR QUALITY CONSIDERATIONS

This section modeled the traffic assignment problem with air quality considerations. A general optimization problem was first formulated. The objective function was established to represent the total travel cost, and the constraints concerned the three requirements of traffic demands, travel speeds, and emission levels. In the case study, the CO was chosen to form the emission constraints and generated the solutions to the optimization problem. The tradeoff between the travel cost and air quality was examined by investigating the optimal objective values given different emission constraints. In addition, two other emissions, NO_2 and O_3, were evaluated under different sets of link volumes.

3.1. Formulation

In this section, the optimization problem was formulated with the objective of the travel cost minimization and the constraints of both the trip and emission requirements. The general formula was shown in Equation (43).

$$\begin{aligned} &\text{Min } f(x) \\ &\text{Subject to } g(x) = b \\ &\qquad h_T(x) <= CT \\ &\qquad h_E(x) <= CE \end{aligned} \tag{43}$$

where

x: a vector representing the path volumes given O-D pairs;

$f(x)$: a function of x representing the total travel cost;

$g(x)$: a set of functions of x representing the traffic distributions;

$h_T(x)$: a set of functions of x representing the travel speeds (or travel times);

$h_E(x)$: a set of functions of x representing the emission levels;

b: a vector representing the O-D pairs;

CT: a vector representing the travel requirements (travel speeds or times); and

CE: a vector representing the emission requirements.

In the above formula, the path volumes under given O-D pairs are the decision variables. In

the constraints, the number of elements in the vectors *b*, *CT*, and *CE* (i.e., the number of functions in *g*, h_T, and h_E) is dependent on the number of O-D pairs, links, and locations where the emission levels are under study. To explicate each of these functions, the notation is first presented.

3.1.1. Notation

$G = (N, L)$: a transportation network;
N: a set of nodes;
L: a set of links;
n: a typical node;
l: a typical link;
W: a set of O-D pairs;
w: a typical O-D pair;
P: a set of paths in the network;
p: a typical path;
P_w: a set of paths connecting O-D pair w;
(A, B): a set of average coordinates of cells after dividing the study area into cells;
(a, b): any typical coordinate; and
(i, j): a typical coordinate of an interesting location.

3.1.2. Total Cost *f(x)*

Normally, the Bureau of Public Roads (BPR) function is adopted to estimate the total cost in transportation planning. As shown in Equation (44), BPR-function recognizes traffic cost (travel time) as an exponential function of roadway loading (volume/capacity, i.e., v/c). The primary objective of this subsection is to connect link volumes with path volumes, which is realized by using Equation (45). Therefore, the total cost *f(x)* can be expressed in Equation (46) in terms of the path volumes.

$$T_f = T_0\left[1 + \alpha\left(\frac{v}{c}\right)^{\beta}\right] \tag{44}$$

where

T_f : travel cost;

T_0 : travel cost without volumes;

$\frac{v}{c}$: v/c ratio, i.e., roadway loading; and

α and β : coefficients given different road types and speed limits.

$$v_l = \sum_{p \in P} x_p \delta_{l,p} \tag{45}$$

where

x_p : volume in path *p*; and

$\delta_{l,p}$: an indicator. If link *l* is contained in path *p*, $\delta_{l,p}$ = 1, and 0, otherwise.

$$f(x) = \sum_{l \in L} T_{0l} \left[1 + \alpha_l \left(\frac{v_l}{c_l} \right)^{\beta_l} \right] = \sum_{l \in L} T_{0l} \left[1 + \alpha_l \left(\frac{\sum_{p \in P} x_p \delta_{l,p}}{c_l} \right)^{\beta_l} \right] \tag{46}$$

3.1.3. Traffic Demand *g(x)*

The constraint of the traffic demand means that the summation of the path volumes is equal to the total demand of the corresponding O-D pair, as shown in Equation (47).

$$g(x) = \sum_{p \in P_w} x_p = b_w \tag{47}$$

where b_w is demand in the O-D pair *w*.

3.1.4. Travel Requirement $h_T(x)$

The objective of the travel requirement is to constrain the link/path travel cost to below an accepted level. Equation (48) and Equation (49) consider the link and path travel cost, respectively.

$$\frac{T_{f,l}}{Ln_l} <= CT_l \tag{48}$$

$$\frac{\sum_{l\ in\ p} T_{f,l}}{\sum_{l\ in\ p} Ln_l} <= CT_p \tag{49}$$

where

Ln_l : length of link l; and

CT_l or CT_p: requirement for a particular link or path. These two may vary by links or paths.

3.1.5. Emission Requirement $h_E(x)$

Similar to the travel requirement, the objective of emission requirement is to constrain the emissions in any location to below an accepted level. The entire study area is divided into cells. The commonly used method to estimate this cell-based emission impact is the Gaussian model in environmental engineering (Ott, 1995; Weiner and Matthews, 2002). The original format of the Gaussian model is:

$$e(x,y,z) = \frac{Q}{2\pi u\sigma_y\sigma_z}\exp\left(-\frac{y^2}{2\sigma_y^2}\right)\left(\exp\left(-\frac{(z+H)^2}{2\sigma_z^2}\right)+\exp\left(-\frac{(z-H)^2}{2\sigma_z^2}\right)\right) \tag{50}$$

where

$e(x,y,z)$: emission concentration at some point in space with coordinate (x, y, z);

Q : emission rate of the pollution source;

u : average wind speed;

σ_y : standard deviation in the y direction;

σ_z : standard deviation in the z direction; and

H : height of the emission source.

In this study, we have the following considerations:

1. The heights for both the emission source and the study location are assumed to be 0, i.e., $z = 0$, $H = 0$.

2. Only when the source cell (*a, b*) is in the upstream of the target cell (*i, j*) along the direction of the wind can the emission be transferred from cell (*a, b*) to cell (*i, j*); otherwise, there is no emission impact from cell (*a, b*) on cell (*i, j*).
3. The ground-level coordinates are derived from the locations of both the emission source cell (*a, b*) and target cell (*i, j*), e.g., $x = (a - i) * d_C$, $y = (b - j) * d_C$. Given the ground-level coordinates, σ_y and σ_z can be estimated according to the wind speed.
4. The emission rate in the emission source cell (*a, b*) in terms of gram per second (g/s) is a function of different traffic conditions, which can also be derived from the link volume and speed, i.e., $Q = q(v_l)$.

Therefore, when estimating the emission impact of cell (*a, b*) on cell (*i, j*), the general Gaussian model is reduced to be:

$$e(i, j, a, b) = \begin{cases} \dfrac{q(v_l)}{\pi u \sigma_y((a-i)d_C)\sigma_z(a-i)d_C)} \exp\left(-\dfrac{((b-j)d_C)^2}{2(\sigma_y(a-i)d_C)^2}\right) = q(v_l) * Ge(a,b) \\ \\ 0 \end{cases} \tag{51}$$

where $Ge(a,b) = \dfrac{1}{\pi u \sigma_y((a-i)d_C)\sigma_z(a-i)d_C)} \exp\left(-\dfrac{((b-j)d_C)^2}{2(\sigma_y(a-i)d_C)^2}\right)$, representing a coefficient based on the geometric relationship between cell (*a, b*) and cell (*i, j*).

And the emission requirement can be expressed in the following:

$$\sum_{(a,b)\in(A,B)} e(i, j, a, b) = \sum_{(a,b)\in(A,B)} q(v_l) * Ge(a,b) <= CE_{(a,\,b)} \tag{52}$$

where $CE_{(a,\,b)}$ is the requirement for particular location. It may vary from cells.

3.2. Case Study

This section describes a case study that was conducted on a network in College Station, Texas. The structure of the network was first described, including the geometries, O-Ds, and road

conditions. Then variables and parameters in the formulations presented in the previous section were discussed. Matlab was used to solve the optimization problem.

3.2.1. Structure of the Network

Figure 20 shows the network in Google Earth and the abstracted network with grids. The cell size is 0.25 mi by 0.25 mi. The detailed information, including the road name, lane number, length, and O-D matrix, is summarized in Table 7.

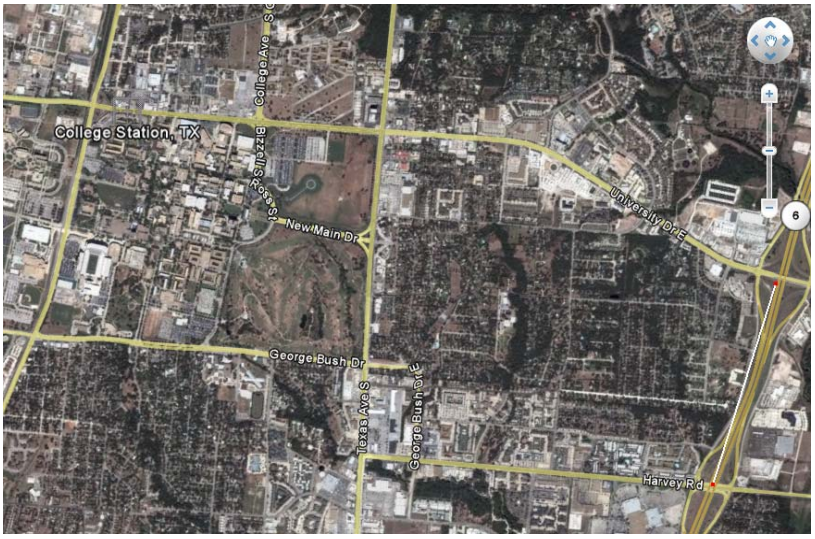

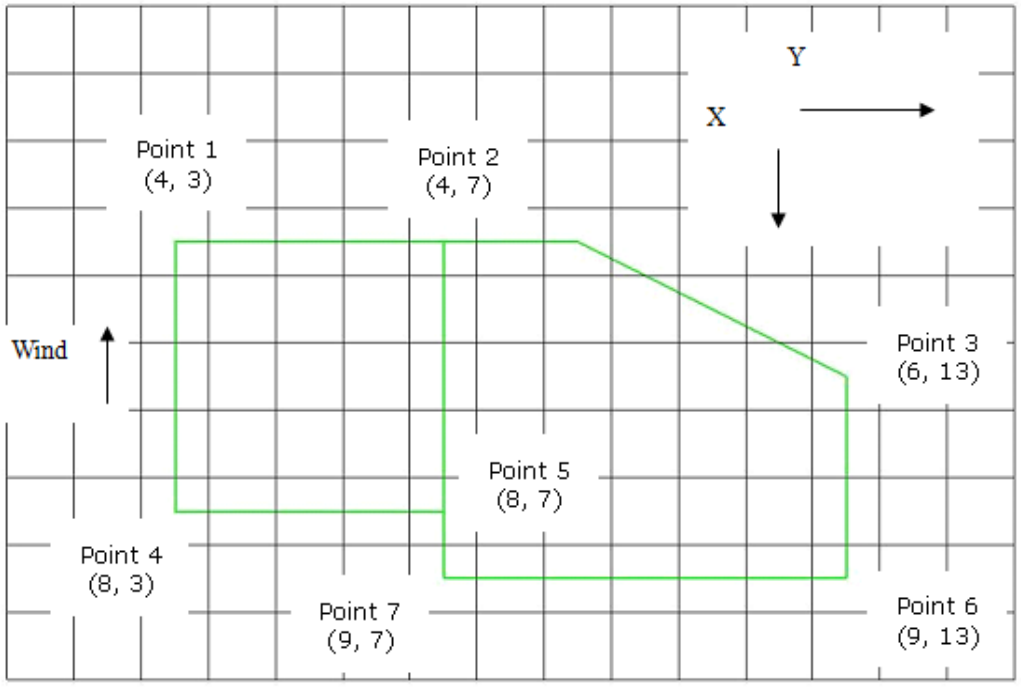

Figure 20. Network in the case study

Table 7. Road condition of each link in the network and O-D pairs

Link	Name	# of Lanes	Length (miles)
L: 1-2	University Dr.	6	1.00
L: 2-3	University Dr.	6	1.62
L: 1-4	Wellborn Rd.	4	1.00
L: 2-5	Texas Ave.	6	1.25
L: 3-6	H6 Frontage	4	0.75
L: 4-7	G. Bush Dr.	4	1.00
L: 7-6	Harvey Rd.	4	1.50

O-D	1	2	3	4	5	6
1		818	407	698	324	565
2	1228	0	1088	454	787	354
3	610	726	0	436	447	156
4	465	454	291	0	698	265
5	324	1180	447	698	0	446
6	377	532	235	397	670	0

3.2.2. Variables and Parameters

Path Volumes

In a traffic assignment problem, the computation load increases dramatically with the increase in the number of nodes and links considered. For example, in the case study, a total of over 100 possible paths could be assigned on 7 links for a given O-D matrix. Based on the geometry of the network, we selected 74 of them as the decision variables for the optimization problem. Table 8 shows the list of one-directional paths. The total number of these paths is 37 = 74/2.

Table 8. Paths in the network (decision variables)

O-D pair	Path	Number of paths
1-2	1-2, 1-4-5-2	2
1-3	1-2-3, 1-2-5-6-3, 1-4-5-2-3, 1-4-5-6-3	4
1-4	1-2-5-4, 1-4,	2
1-5	1-2-5, 1-4-5	2
1-6	1-2-3-6, 1-2-5-6, 1-4-5-6	3
2-3	2-3, 2-5-6-3	2
2-4	2-1-4, 2-5-4	2
2-5	2-1-4-5, 2-3-6-5, 2-5	3
2-6	2-3-6, 2-5-6	2
3-4	3-2-1-4, 3-2-5-4, 3-6-5-4	3
3-5	3-2-5, 3-6-5	2
3-6	3-6, 3-2-5-6	2
4-5	4-1-2-5, 4-5	2
4-6	4-1-2-3-6, 4-1-2-5-6, 4-5-2-3-6, 4-5-6	4
5-6	5-2-6, 5-6	2
	Total	37

Travel Time

Considering that all the roads in the network are either urban arterials or freeway frontage roads, a free-flow speed of 50 mph was used for all links in the case study. To compute the objective value, we selected the typical parameters for BPR function (Traffic Engineering, 2009): $\alpha = 0.71$ and $\beta = 2.10$. For the travel requirement, CT = 1/(35 mph); that is, the average speeds shouldn't be less than 35 mph.

Emission

This study used CO to form the emission constraint in the optimization problem (Yin and Lawphongpanich, 2006; Lin and Ge, 2006). The emission rate was estimated by MOBILE 6.2 to conduct the case study. The scenario was designed for winter months with the temperature ranging from 40 to 45°F. Wind was assumed to be 18 ft/s (about 12 mph), with the direction shown in Figure 20. The σ_y and σ_z in Equation (51) were calculated

according to the atmospheric stability at class C.

The emission rate output directly by MOBILE 6.2 is in terms of gram per vehicle per mile (g/veh/mile), which can be converted to gram per vehicle per second (g/veh/s). Table 9 summarizes the relationship between speeds and emission rates. This relationship, along with the traffic stream model, can determine the relationship between the traffic volume and emission rate. A simple relationship is assumed between speed and density. This assumption is commonly used in traffic flow analysis and provided sufficient accuracy for this study. The jam density was set to be 120 vehicles per mile per lane (vpmpl), and the free-flow speed was 50 mph. The density was also implicitly considered by computing the total emission rate from all the vehicles in a one mi road segment. Figure 21 shows the relationship between volumes and emission rates in terms of g/mile/s at different free-flow conditions. Similar to the volume vs. speed chart, the volume vs. emission rate chart had two emission rate values corresponding to a single volume value. For either branch of the two in this chart (Figure 21), the relationship was close to linear. In this study, we only considered the uncongested condition for planning purposes. The regression analysis was conducted (Table 10), and the large R-square value supported the linear relationship.

Table 9. Relationship between speed and emission rate

Speed	Emission Rate	
(mph)	(g/veh/mile)	(g/veh/s)
5	24.62	0.034194
10	17.97	0.049917
15	16.01	0.066708
20	15.02	0.083444
25	14.49	0.100625
30	14.25	0.11875
35	14.3	0.139028
40	14.77	0.164111
45	15.23	0.190375
50	15.7	0.218056
55	16.16	0.246889
60	16.62	0.277
65	17.09	0.308569

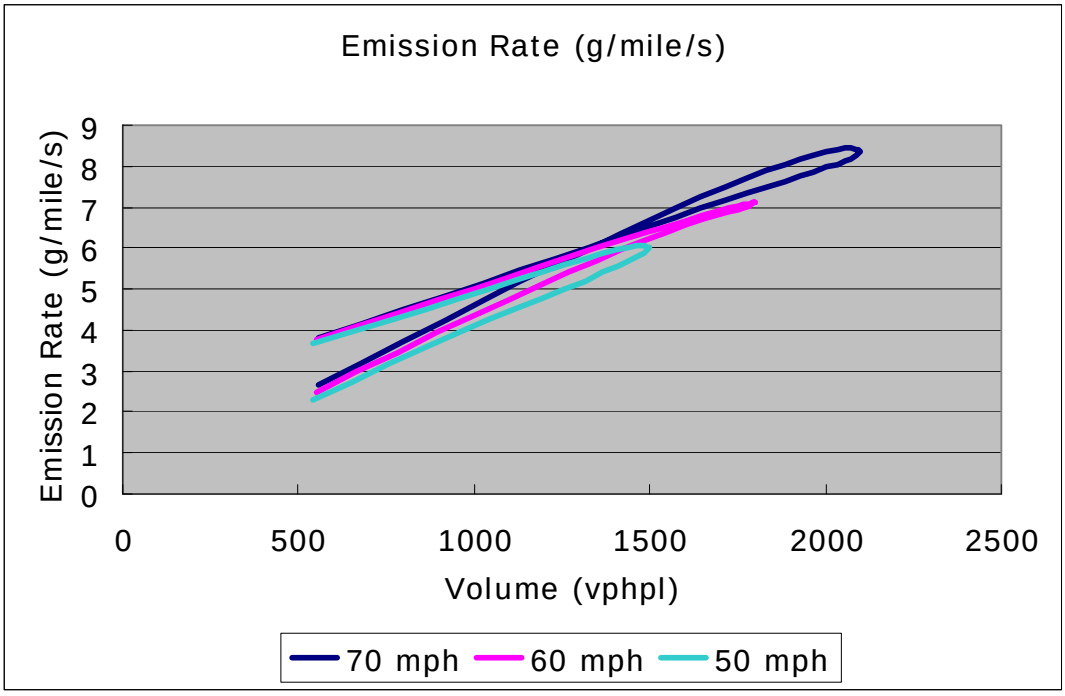

Figure 21. Relationship between volume and emission rate

Table 10. Regression analysis of the relationship between volume and emission rate

Regression Result	70 mph	60 mph	50 mph
Intercept	0.7855	0.5541	0.2172
Slope	0.0038	0.0037	0.0038
R-Square	0.9888	0.9955	0.9990

3.2.3. Solver

All the functions involved in the optimization problem were linear except the BPR function, and the BPR function was convex in nature. The optimization toolbox in Matlab was used to solve the convex problem. The program was run on a personal computer, with a processor of Inter(R) Pentium(R) Dual CPU T2310 @ 1.46GHz 1.47 GHz with a memory (RAM) of 3070 MB. The optimal solution was produced within half a minute.

3.2.4. Results

Figure 22 shows the results including the optimal solution, objective values, and maximum

constraint violations along with the number of iterations, with *CE* in an ascending order. If the value of the maximum constraint violations is much smaller than the absolute constraint value, the maximum constraint violations can be considered 0. When the maximum constraint violations can't reach 0 (i.e., Figure 22[g]), it means that no matter how the traffic is assigned in the network, the combined requirement from both the travel cost and air quality can't be fulfilled. In this case study, we found that the emission requirement cannot be less than or equal to 0.24 ppm. Figure 23 illustrates the tradeoff between the total travel time and the emission requirement (i.e., *CE*). As *CE* goes up (i.e., the emission requirement becomes lower), the total travel time decreases. Moreover, this decrease rate decreases as *CE* goes up, and reaches 0 after *CE* = 0.30 ppm, meaning that the emission requirement (*CE*) won't affect the optimization problem anymore. Figure 23 also supports the concept of relocating traffic to improve the air quality. For the extreme case, the air quality is improved by 16.7% = (0.30 – 0.25) / 0.30 with the increase of the total travel time of 10.3% = (683 – 619) / 619. This benefit is even more apparent if the air quality is improved by 13.3% = (0.30 – 0.26) / 0.30 with the increase of the total travel time of just 2.1% = (632 – 619) / 619.

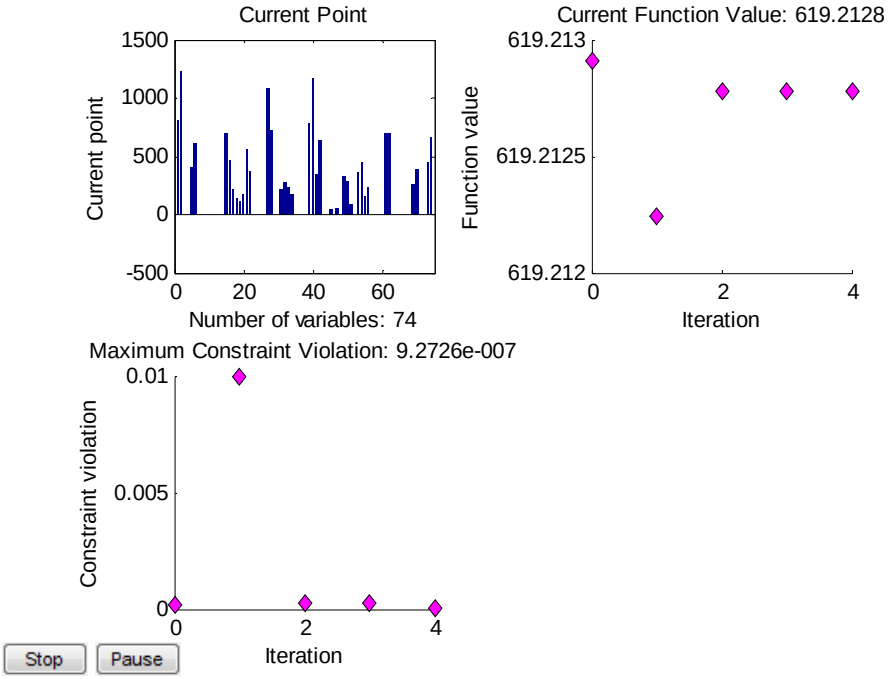

(a) *CE* = 0.30 ppm

Figure 22. Optimal solutions produced by Matlab

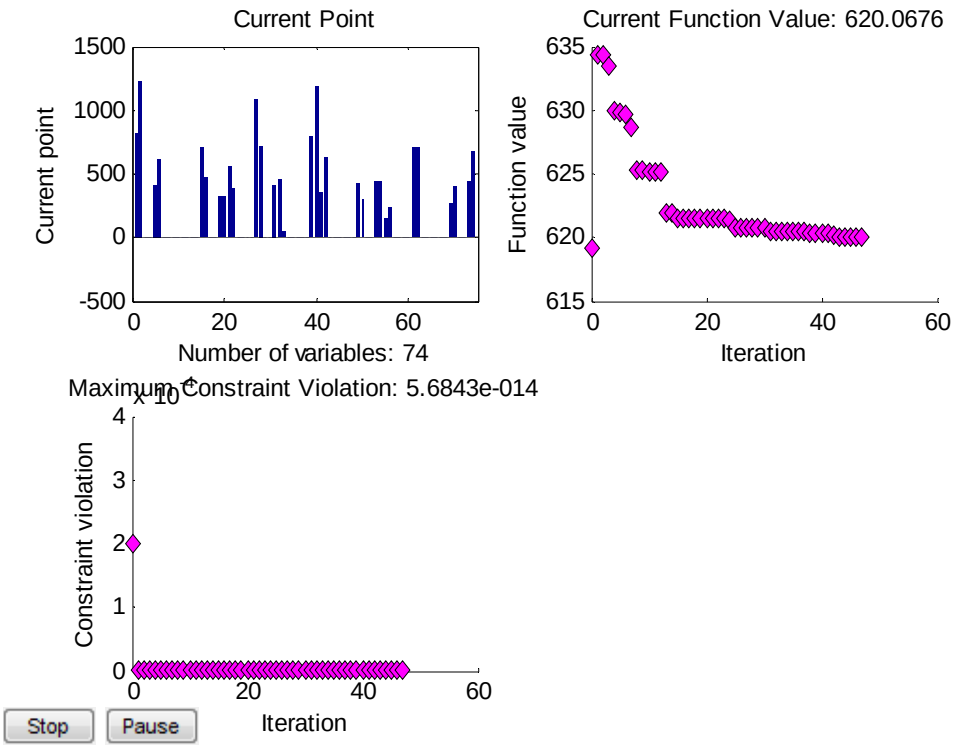

(b) *CE* = 0.29 ppm

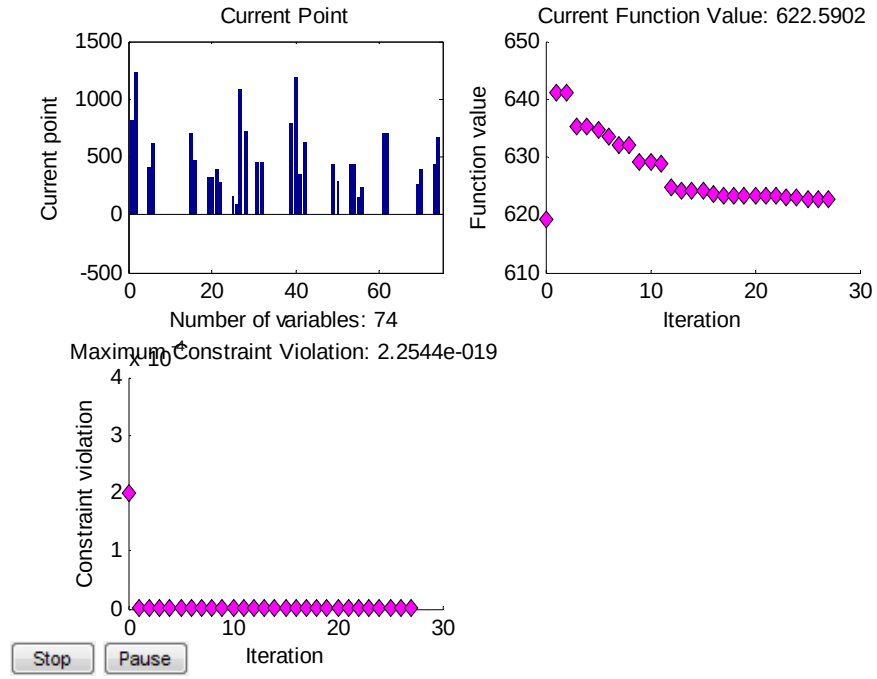

(c) *CE* = 0.28 ppm

Figure 22 (continued). Optimal solutions produced by Matlab

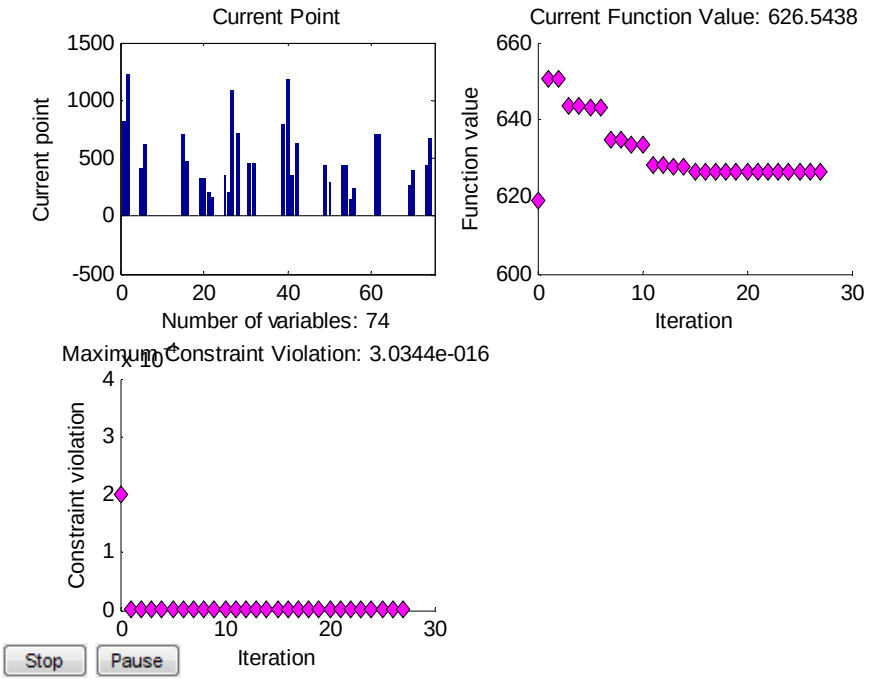

(d) *CE* = 0.27 ppm

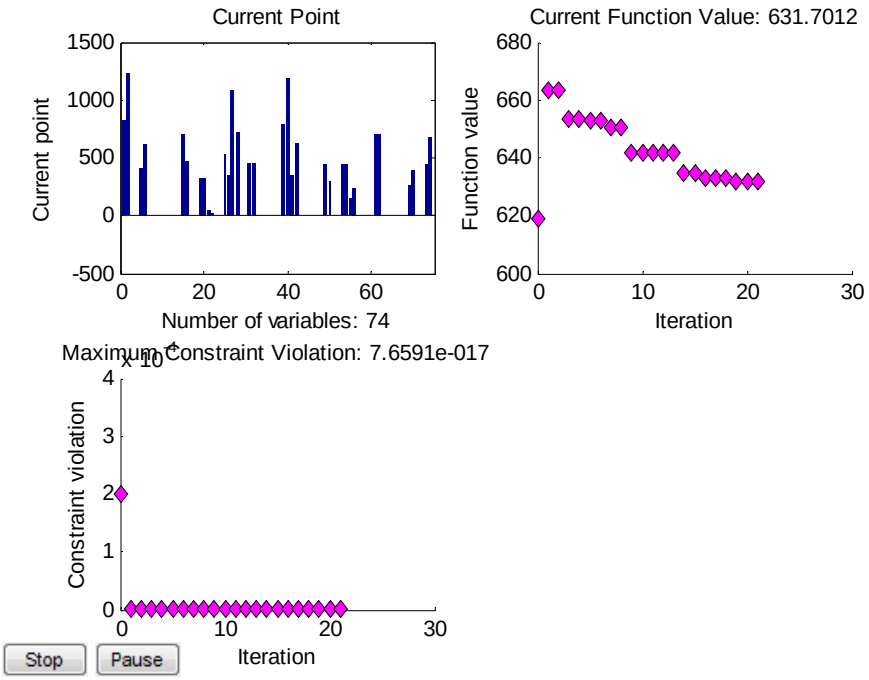

(e) *CE* = 0.26 ppm

Figure 22 (continued). Optimal solutions produced by Matlab

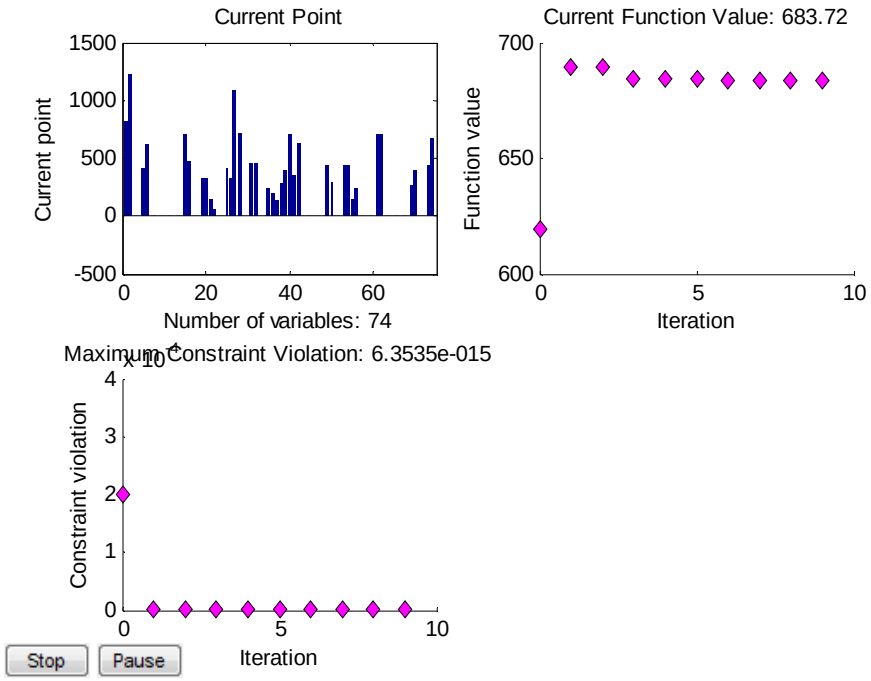

(f) *CE* = 0.25 ppm

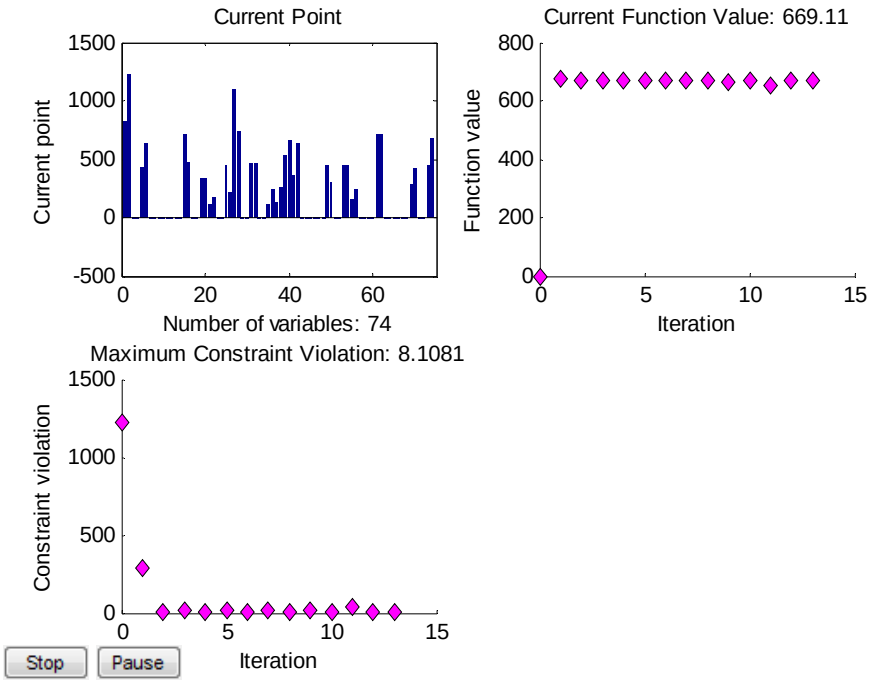

(g) *CE* = 0.24 ppm

Figure 22 (continued). Optimal solutions produced by Matlab

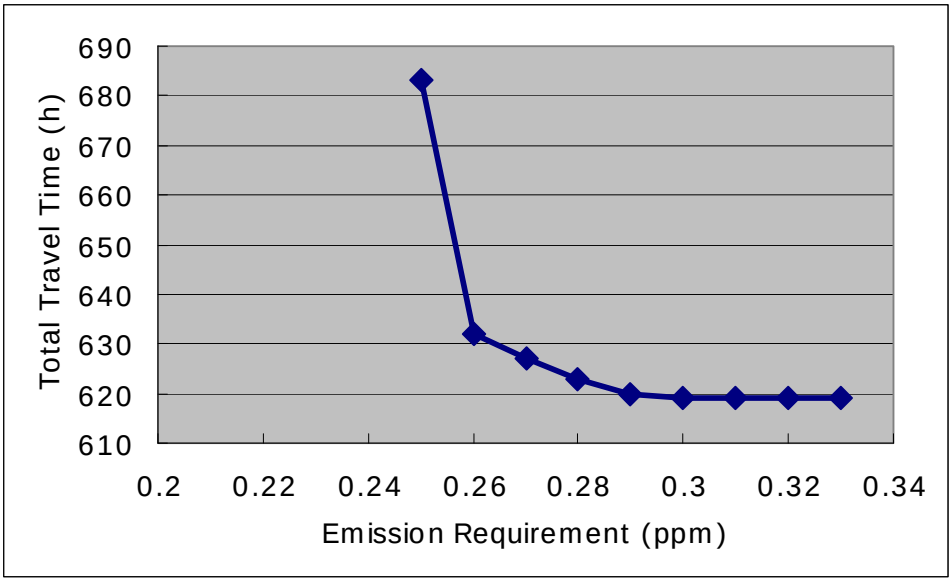

Figure 23. Tradeoff between the total travel time and the emission requirement

Figure 24 shows the comparison of emission contours between *CE* = 0.25 ppm and *CE* = 0.30 ppm. When *CE* = 0.30 ppm, the maximum emission happens at point 2. The traffic on links 2-5 and 5-2 make a significant contribution to this highest emission value. So as the emission requirement increases (as *CE* decreases), the traffic flows on links 2-5 and 5-2 are reassigned to alternative links. As shown in Figure 25, which describes the changes of 14 link volumes with an increase in the emission requirement, the traffic volumes on both link 2-5 and link 5-2 increase as *CE* decreases. However, as *CE* decreases, links 1-4 and 4-1, which are parallel to links 2-5 and 5-2, contain more traffic and consequently involve higher emission levels.

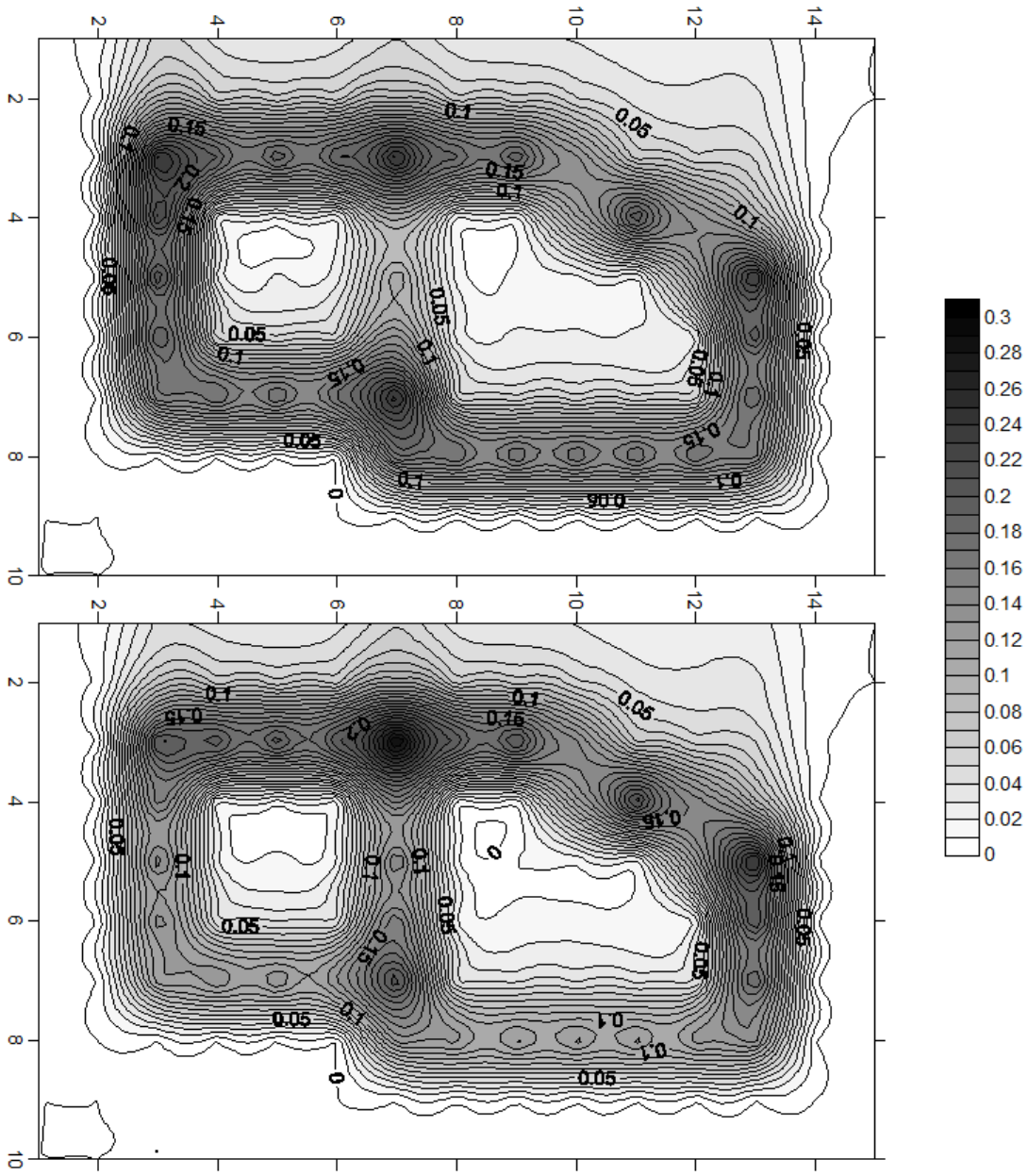

Figure 24. Comparison of emission contours between *CE* = 0.25 ppm (upper) and *CE* = 0.30 ppm (lower)

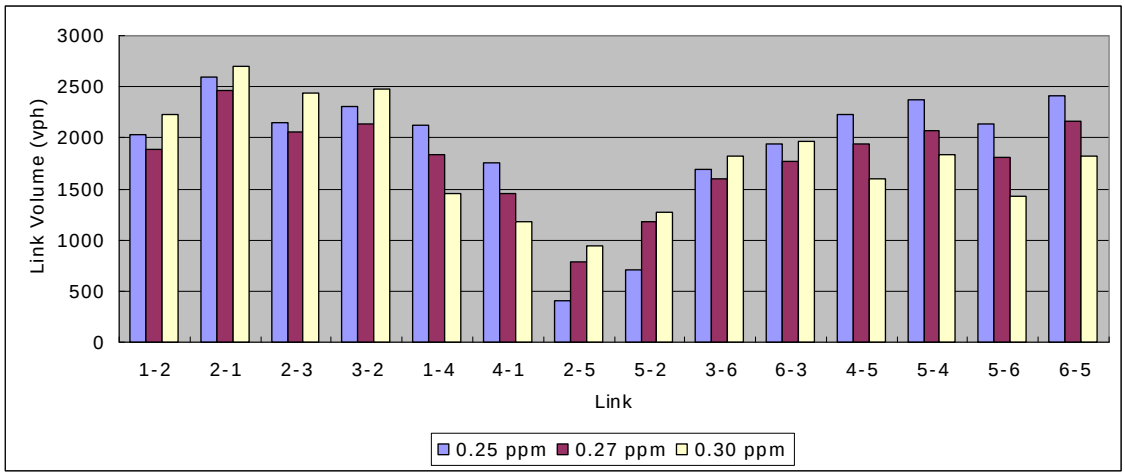

Figure 25. Link volumes under different *CE*s (0.25, 0.27, and 0.30 ppm)

One of the most important advantages of this study over the previous ones is that the proposed model could estimate the emission levels in any location, not only on the road but also in the surrounding areas. With this, different emission requirements can be assigned for different locations or different objects. In the study network, cell (7, 7) contains a commercial plaza and usually involves a high density of people. Cell (7, 7) is considered a vulnerable object and has a higher emission requirement. By setting *CE* (7, 7) at a lower value while keeping *CE*s at the other locations constant at 0.35 ppm, Figure 26 illustrates the tradeoff between the total travel time and the emission requirement (i.e., *CE*) at this vulnerable location in cell (7 ,7). Compared with Figure 23, Figure 26 shows the similar relationship between the total travel time and the emission requirement; as *CE* goes up (i.e., the emission requirement becomes lower), the total travel time decreases, and this decrease rate reaches 0 after *CE* is greater than a threshold value. However, Figure 26 has a lower absolute value of emission requirement than that in Figure 23, because it only focuses on minimizing *CE* at one vulnerable location instead of considering emission requirements for all the cells in the entire study area.

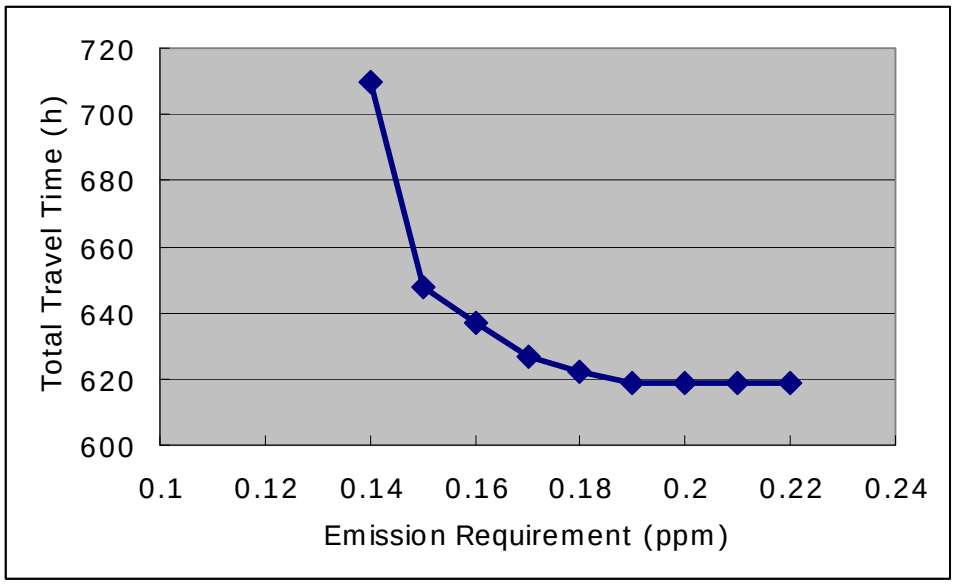

Figure 26. Higher emission requirements for a vulnerable object in cell (7, 7)

3.3. Evaluation of Multiple Pollutants

Among the pollutants caused by traffic, CO is very stable and usually not involved in any chemical reaction. Compared with the other pollutants, CO concentration is easier to model and predict. Most studies have only investigated the effect of the traffic on CO (Yin and Lawphongpanich, 2006; Lin and Ge, 2006). But in this study, we also compared the contours of two other different pollutions, NO_2 and O_3, which involve chemical reactions to different degrees. As discussed in Section 2.3.1, O_3 involves more chemical reactions than NO_2.

The gas phase chemistry simulation was applied to evaluate the concentrations of NO_2 and O_3 in the study area. Figure 25 presented three sets of link volumes based on different emission requirements (*CE*) of CO. Figure 27 and 28 show the contours of NO_2 and O_3, given each of these three sets of link volumes. Figure 27 illustrates a similar change trend of NO_2 concentrations to the CO concentrations with the decrease of *CE*. As *CE* decreased, the NO_2 concentrations along link 2-5 decreased, and point 1 replaced point 2 to become the location with the highest NO_2 concentration. However, it was difficult to identify the transition of the highest concentration location in the contours of O_3. Due to the complex chemical reflections, the highest O_3 concentration occurred not in the vicinity of roads, but in the locations that

were several miles away from the roads in the downstream of the wind direction. The highest O_3 concentration was more dependent on the total traffic in the study area than the traffic assignment in the network.

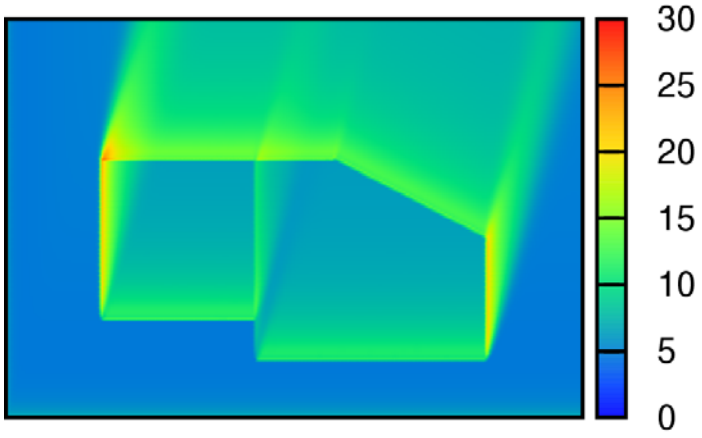

(a) CE = 0.25 ppm

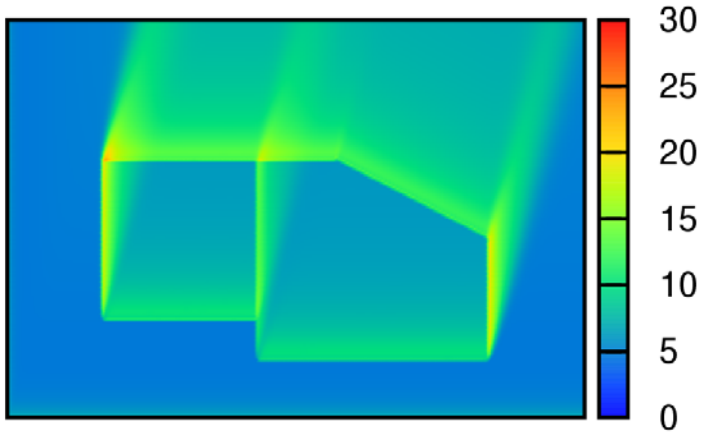

(b) CE = 0.27 ppm

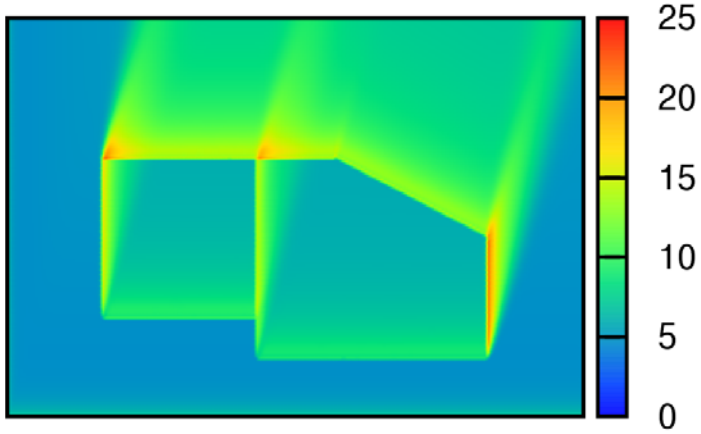

(c) CE = 0.30 ppm

Figure 27. Contours of NO_2 (Unit: 10^3 ppm)

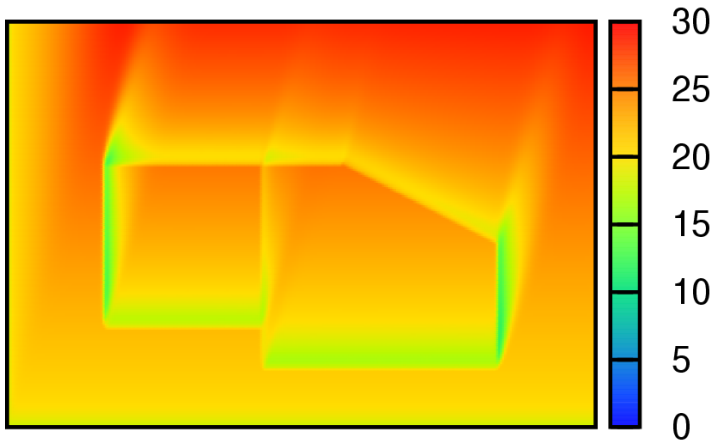

(a) CE = 0.25 ppm

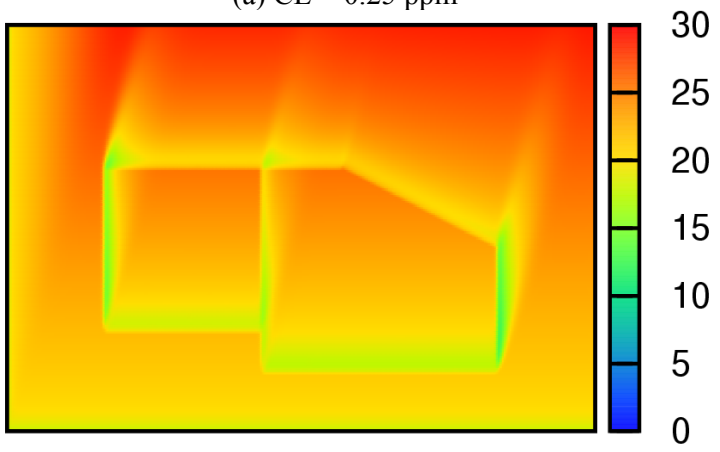

(b) CE = 0.27 ppm

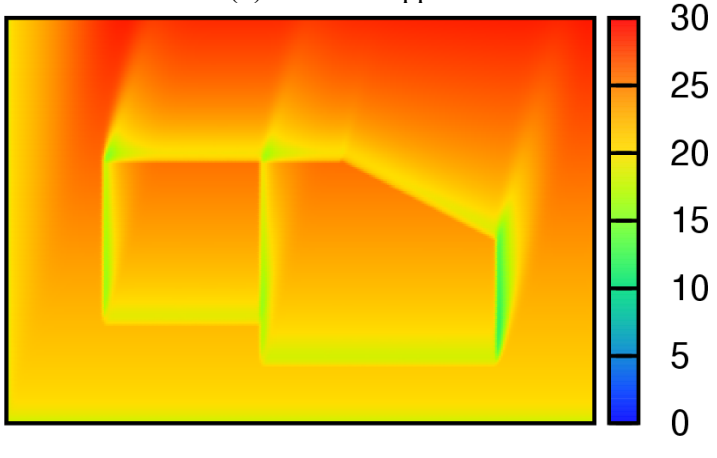

(c) CE = 0.30 ppm

Figure 28. Contours of O_3 (Unit: 10^3 ppm)

4. CONCLUSIONS

This study first modeled the near-road air quality. Both the physical and chemical transformations were considered. The numerical studies suggest that gas phase chemistry is needed to accurately predict the concentration of O_3, NO, NO_2, and BUTA near a busy freeway. The effect of gas phase chemistry on BUTA is less significant when the freeway is in an O_3 depleted location, such as in an urban center, but is quite significant when the freeway is located in a location downwind of the urban ozone plume due to a significant increase in the HO radical concentration. Neglecting the gas chemistry near a freeway will lead to an overestimation ozone concentrations in the downwind direction. In addition, the increase in the HO radical near a freeway may also imply potential health effects due to the strong oxidative power of the radicals.

Second, this study presented a method to assign traffic in an urban network considering constraints of both the traffic demands and air quality. An optimization problem was formulated with path volumes as the decision variables. Normally, it involves a very heavy computation load to solve such an optimization problem, not only because the emission constraint is considered, but also due to the fact that the traffic assignment problem itself is very complicated. To address this problem, reasonable approximations were discussed to make the problem solvable even on a personal computer. Compared with previous studies, the proposed model is able to provide emission estimations for any location in the study area, and it also demonstrates its capability of solving the traffic assignment problem on a large-scale network for the planning purpose. The case study in College Station, Texas, involved 14 links, 30 O-D pairs, and 74 decision variables. The CO emissions were selected to model the air quality requirement. The maximum emission levels were always found near the intersection that contained the most traffic in the study area. The tradeoff between the total travel cost and the air quality was examined by tracking the evolution of the optimal objective value (total travel time) with the change of emission constraints (*CE*). As *CE* went up (i.e., the emission requirement became lower), the total travel time decreased, and the decrease rate reached 0 after *CE* was greater than a threshold value, which means that the emission requirement (*CE*) didn't affect the optimization problem after that. This air quality benefit from relocating traffic was identified by an observed 13.3% reduction in the emission level with only a 2.1% increase in total travel time. When we focused on a local cell instead of all the cells in the study area, the emission level reached a smaller value in the interested

cell, but, accordingly, a larger total travel time in the network was generated.

In addition to CO, NO_2 and O_3 were also evaluated given three different sets of link volumes. Both NO_2 and O_3 are not as stable as CO, and involve some chemical reactions. It needs more chemical reactions to form O_3 than NO_2. Simulation results indicated that NO_2 has a similar trend of the concentration evolution to CO. With a decrease of *CE*, the NO_2 levels in the worst locations (link 2-5 in the case study) decreased. However, there was no significant spatial difference in the highest O_3 concentrations among the three sets of link volumes, because O_3 involves very complex chemical reactions. The highest O_3 concentration usually occurred in the area that was several miles away from the road network. This highest value was more dependent on the total traffic in the study area than the traffic assignment within the network.

Although this study investigated the key issues in the developments of both the near-road dispersion model and the traffic assignment model, it has a few limitations that could be further addressed in future studies. First, the development of both the near-road dispersion model and the traffic assignment model is based on databases (GM and Mobile 6.2 databases) that were established decades ago. Considering the changes in vehicle engines and driver behaviors, it would be very beneficial to collect field data to calibrate and validate the proposed models. Second, our current optimization problem considered only the CO level in the constraint. Although the NO_2 and O_3 levels were also evaluated under different sets of link volumes, different emissions (CO, NO_2, and O_3) could be considered in the optimization problem simultaneously in the future model. Finally, in this study, the method was proposed mainly for the planning purpose. It could be extended for the application at the operations level by improving the estimations of vehicle movements in the network.

REFERENCES

Ahn, K., and Rakha, H. (2008). "The effects of route choice decisions on vehicle energy consumption and emissions." *Transportation Research Part D: Transport and Environment*, 13(3), 151-167.

Balmes, R. J., Gillian, E., Patricia, P. K., Edward, H. Y., Mark, D. E., Hubert, C., Laura, T., Fred, L., and Paul, D. B. (2009). "Exposure to traffic: Lung function and health status in adults with asthma." *The Journal of allergy and clinical immunology*, 123(3), 626-631.

Barth, M. (2007). "Environmentally-friendly navigation." *IEEE Intelligent Transportation Systems Conference*.

Bäumer, D., Vogel, B., and Fiedler, F. (2005). "A new parameterisation of motorway-induced turbulence and its application in a numerical model." *Atmospheric Environment*, 39(31), 5750-5759.

Benedek, C. M., and Rilett, L. R. (1998). "Equitable traffic assignment with environmental cost functions." *Journal of Transportation Engineering*, 124(1), 16-22.

Benson, P. E. (1992). "A review of the development and application of the CALINE3 and 4 models." *Atmospheric Environment Part B: Urban Atmosphere*, 26, 379–390.

Brugge, D. B., Durant, J. L. D., and Rioux, C. (2007). "Near-highway pollutants in motor vehicle exhaust: A review of epidemiologic evidence of cardiac and pulmonary health risks." *Environmental Health*, 6(23).

Cadle, S. H., Chock, D. P., Heuss, J. M., and Monson, P. R. (1978). "Results of the General Motors sulfate dispersion experiment." General Motors Research Laboratories, Warren, MI.

Carter, W. P. L. (2000). "Implementation of the SAPRC-99 chemical mechanism into the models-3 framework." United States Environmental Protection Agency.

Corlella, P., and Woodward, P. R. (1984). "Piecewise parabolic method (PPM) for gas-dynamical simulations." *Journal of Computational Physics*, 54, 174-201.

Darnall, K. R., Lloyd, A. C., Winer, A. M., and Pitts, J. N. (1976). "Reactivity scale for atmospheric hydrocarbons based on reaction with hydroxyl radical." *Environmental Science & Technology*, 10(7), 692-696.

Finkelstein, M. M., Jerrett, M., and Sears, M. R. (2004). "Traffic air pollution and mortality rate advancement periods." *American Journal of Epidemiology*, 160(2), 173–177.

Gauderman, W. J., Vora, H., McConnell, R., Berhane, K., Gilliland, F., Thomas, D., Lurmann, F., Avol, E., Kunzli, N., Jerrett, M., and Peters, J. (2007). "Effect of exposure to traffic on lung development from 10 to 18 years of age: a cohort study." *The Lancet*, 369(9561), 571-577.

Grosjean, D., Grosjean, E., and Gertler, A. W. (2000). "On-road emissions of carbonyls from light-duty and heavy-duty Vehicles." *Environmental Science & Technology*, 35(1), 45-53.

Held, T., Chang, D. P. Y., and Niemeier, D. A. (2003). "UCD 2001: an improved model to simulate pollutant dispersion from roadways." *Atmospheric Environment*, 37(38), 5325-5336.

Holmes, N. S., and Morawska, L. (2006). "A review of dispersion modelling and its application to the dispersion of particles: An overview of different dispersion models available." *Atmospheric Environment*, 40(30), 5902-5928.

Jacobson, M. Z. (2005). *Fundamentals of atmospheric modeling*, Cambridge University Press, Cambridge, UK.

Kean, A. J., Harley, R. A., Littlejohn, D., and Kendall, G. R. (2000). "On-Road measurement of ammonia and other motor vehicle exhaust emissions." *Environmental Science & Technology*, 34(17), 3535-3539.

Kim, J. J., Smorodinsky, S., Lipsett, M., Singer, B. C., Hodgson, A. T., and Ostro, B. (2004). "Traffic-related air pollution near busy roads: The east bay children's respiratory health study." *American Journal of Respiratory and Critical Care Medicine*, 170(5), 520-526.

Kinnee, E. J., Touma, J. S., Mason, R., Thurman, J., Beidler, A., Bailey, C., and Cook, R. (2004). "Allocation of onroad mobile emissions to road segments for air toxics modeling in an urban area." *Transportation Research Part D: Transport and Environment*, 9(2), 139-150.

Levy, H., II. (1971). "Normal atmosphere: large radical and formaldehyde concentrations predicted." *Science*, 173(3992), 141-143.

Lin, J., and Ge, Y. E. (2006). "Impacts of traffic heterogeneity on roadside air pollution

concentration." *Transportation Research Part D: Transport and Environment*, 11(2), 166-170.

McRae, G. J., and Seinfeld, J. H. (1983). "Development of a second-generation mathematical model for urban air pollution--II. Evaluation of model performance." *Atmospheric Environment (1967)*, 17(3), 501-522.

Monin, A. S., and Obukhov, A. M. (1954). "Basic laws of turbulent mixing in the ground layer of the atmosphere." *Trudy Geofiz. Inst. Akad. Nauk SSSR*, 24, 163-187.

Morrow, N. L. (2001). "Significance of 1,3-butadiene to the US air toxics regulatory effort." *Chemico-Biological Interactions*, 135-136, 137-143.

Murena, F. (2007). "Air quality nearby road traffic tunnel portals: BTEX monitoring." *Journal of Environmental Sciences*, 19(5), 578-583.

Nagurney, A. (2000). "Alternative pollution permit systems for transportation networks based on origin/destination pairs and paths." *Transportation Research Part D: Transport and Environment*, 5(1), 37-58.

Nagurney, A. (2000). "Congested urban transportation networks and emission paradoxes." *Transportation Research Part D: Transport and Environment*, 5(2), 145-151.

Nagurney, A., Ramanujam, P., and Dhanda, K. K. (1998). "A multimodal traffic network equilibrium model with emission pollution permits: compliance vs noncompliance." *Transportation Research Part D: Transport and Environment*, 3(5), 349-374.

Niemeier, U., Granier, C., Kornblueh, L., Walters, S., and Brasseur, G. P. (2006). "Global impact of road traffic on atmospheric chemical composition and on ozone climate forcing." *J. Geophys. Res.*, 111(D9), D09301.

Ntziachristos, L., Ning, Z., Geller, M. D., Sheesley, R. J., Schauer, J. J., and Sioutas, C. (2007). "Fine, ultrafine and nanoparticle trace element compositions near a major freeway with a high heavy-duty diesel fraction." *Atmospheric Environment*, 41(27), 5684-5696.

Ott, W. (1995). *Environmental statistics and data analysis*, Lewis Publisher.

Press, W. H., Teukolsky, S. A., Vetterling, W. T., and Flannery, B. P. (1992). *Numerical recipes in FORTRAN. The art of scientific computing*, Cambridge: University Press.

Rao, K. S. (2002). "ROADWAY-2: A model for pollutant dispersion near highways." *Water,*

Air, & Soil Pollution: Focus, 2(5), 261-277.

Rao, S. T., Sistla, G., Eskridge, R. E., and Petersen, W. B. (1986). "Turbulent diffusion behind vehicles: Evaluation of ROADWAY models." *Atmospheric Environment (1967)*, 20(6), 1095-1103.

Richmond-Bryant, J., Saganich, C., Bukiewicz, L., and Kalin, R. (2009). "Associations of PM2.5 and black carbon concentrations with traffic, idling, background pollution, and meteorology during school dismissals." *Science of The Total Environment*, 407(10), 3357-3364.

Sahlodin, A. M., Sotudeh-Gharebagh, R., and Zhu, Y. (2007). "Modeling of dispersion near roadways based on the vehicle-induced turbulence concept." *Atmospheric Environment*, 41(1), 92-102.

Sehmel, G. A. (1973). "Particle resuspension from an asphalt road caused by car and truck traffic." *Atmospheric Environment (1967)*, 7(3), 291-309.

Seiber, J. N. (1996). "Toxic air contaminants in urban atmospheres: Experience in California." *Atmospheric Environment*, 30(5), 751-756.

Seinfeld, J. H., and Pandis, S. N. (2006). *Atmospheric chemistry and physics -From air pollution to climate change*, John Wiley & Sons.

Stull, R. B. (1988). *An introduction to the boundary layer meteorology*, Kluwer Academic Publishers.

Traffic Engineering: Planning for traffic loads, http://www.sierrafoot.org/local/gp/engineering.html (Last access: November 2009).

U.S. EPA. (2009). "US greenhouse gas emission inventory report." U.S. Environmental Protection Agency.

Venkatram, A. (2004). "On estimating emissions through horizontal fluxes." *Atmospheric Environment*, 38(9), 1337-1344.

Venkatram, A., Isakov, V., Thoma, E., and Baldauf, R. (2007). "Analysis of air quality data near roadways using a dispersion model." *Atmospheric Environment*, 41(40), 9481-9497.

Venn, A. J., Lewis, S. A., Cooper, M., Hubbard, R., and Britton, J. (2001). "Living near a main road and the risk of sheezing illness in children." *American Journal of*

Respiratory and Critical Care Medicine, 164(12), 2177-2180.

Wade, J., Holman, C., and Fergusson, M. (1994). "Passenger car global warming potential: Current and projected levels in the UK." *Energy Policy*, 22(6), 509-522.

Weiner, R., and Matthews, R. (2002). *Environmental engineering*, Butterworth-Heinemann Publisher.

Yin, Y., and Lawphongpanich, S. (2006). "Internalizing emission externality on road networks." *Transportation Research Part D: Transport and Environment*, 11(4), 292-301.

Young, T. R., and Boris, J. P. (1977). "A numerical technique for solving stiff ordinary differential equations associated with the chemical kinetics of reactive-flow problems." *The Journal of Physical Chemistry*, 81(25), 2424-2427.

Zhu, Y., Hinds, W. C., Kim, S., Shen, S., and Sioutas, C. (2002). "Study of ultrafine particles near a major highway with heavy-duty diesel traffic." *Atmospheric Environment*, 36(27), 4323-4335.